Relaxation method for detonations in condensed explosives with pressure–temperature-equilibrium models and Mie–Grüneisen type equations of state

Alexandre Chiapolino, Richard Saurel

▶ **To cite this version:**

Alexandre Chiapolino, Richard Saurel. Relaxation method for detonations in condensed explosives with pressure–temperature-equilibrium models and Mie–Grüneisen type equations of state. Physics of Fluids, 2025, 37 (1), pp.016135. 10.1063/5.0248890 . hal-04904322

HAL Id: hal-04904322
https://hal.science/hal-04904322v1

Submitted on 21 Jan 2025

HAL is a multi-disciplinary open access archive for the deposit and dissemination of scientific research documents, whether they are published or not. The documents may come from teaching and research institutions in France or abroad, or from public or private research centers.

L'archive ouverte pluridisciplinaire **HAL**, est destinée au dépôt et à la diffusion de documents scientifiques de niveau recherche, publiés ou non, émanant des établissements d'enseignement et de recherche français ou étrangers, des laboratoires publics ou privés.

Relaxation method for detonations in condensed explosives with pressure-temperature-equilibrium models and Mie-Grüneisen type equations of state

Alexandre Chiapolino[1a], Richard Saurel[2a,b]

[a] *RS2N SAS, 371 chemin de Gaumin, Saint-Zacharie 83640, France*
[b] *CNRS, Centrale Marseille, Aix Marseille Univ, LMA UMR 7031, Marseille, France*

Abstract

This paper deals with detonation waves in condensed explosives in the context of pressure and temperature equilibrium models. Most engineering solvers for detonation waves in condensed explosives are based on the reactive Euler equations, which model flows evolving in both temperature and pressure equilibrium conditions. Although the assumption of thermal equilibrium is physically questionable, the reactive Euler equations remain the most popular model because of its convenience. Conventional methods rely on Mie-Grüneisen equations of state (EOS) and are challenged by their limited applicability, high computational complexity, and frequent failure. A previous publication addressed these issues by using the Noble-Abel-stiffened-gas EOS as a predictor, followed by a relaxation step to map the solution to the physical target EOS. This novel thermodynamic relaxation framework was originally introduced in the context of mechanical equilibrium. The present work builds on this novel method to encompass both mechanical and thermal equilibrium, thus enabling the treatment of detonation waves in condensed explosives within the framework of pressure and temperature equilibrium models. The proposed method is capable of treating both interfacial flows through "diffuse interface" formulations, and mixture flows in mechanical and thermal equilibrium. In addition, the proposed method demonstrates improved computational robustness, a significant increase in efficiency, and greater flexibility.

Keywords: Shock and detonation waves, Equations of state, Relaxation, Mechanical and thermal equilibrium.

[1]Corresponding author: alexandre.chiapolino@rs2n.eu
[2]richard.saurel@univ-amu.fr

1. Introduction

Most engineering computations dealing with condensed energetic materials use the reactive Euler equations with a mixture equation of state based on temperature and pressure equilibrium among the phases. This system includes the three conventional balance equations of mass, momentum, and energy for the mixture, as well as mass balance equations to describe the chemical composition of the mixture. The model assumes that the mixture evolves with a single temperature as it involves a single energy balance equation. This assumption is reminiscent of gas detonation modeling. However, the assumption of temperature equilibrium between the phases is questionable for detonations of condensed explosives. This is because the mixture is not molecular. The reaction zone is a mixture of multiple phases where mixing occurs at a scale larger than the molecular one. Therefore, assuming thermal equilibrium is doubtful (Kapila et al., 2001 [1], Petitpas et al., 2009 [2], Saurel et al., 2017 [3], Chiapolino et al., 2024 [4]).

However, the reactive Euler equations, with a thermodynamic closure based on temperature and pressure equilibrium conditions, continue to be the most popular model in detonation solvers for a number of reasons. The initial rationale is grounded in an analysis of the involved physics. The measurement of heat exchanges between the solid reactant and the detonation products appears to be impossible due to the limitations imposed by the pressure, density, and temperature conditions, as well as the timescales involved. This is particularly the case with respect to the heat exchange coefficient. This issue is circumvented when thermal equilibrium is assumed, as the exchange coefficient is no longer needed. Furthermore, the reactive Euler equations constitute a conservative system of hyperbolic equations, and the shock relations are well-defined. The reactive Euler equations are employed for convenience and represent the most straightforward approach for addressing detonation waves. The rate of creation of the detonation products is determined by the kinetics of decomposition, which is adjusted with this specific flow model and associated equations of state (EOS) in order to match experimental data. This model assumes that the reactant and the detonation products are always in pressure and temperature equilibrium. It has been used in numerous research contributions, including but not limited to [5–15]. The reactive Euler equations are also extensively used in commercial codes, such as AUTODYN [16] and LS-DYNA [17], to address detonations of condensed explosives.

The reactive Euler equations with temperature and pressure equilibrium among the phases are commonly used to address detonations in condensed explosives due to their convenience. However, their simplicity has limitations and masks a subtle complexity that can lead to pathological detonations. This issue has recently been examined in Chiapolino et al. (2024) [4] where a fundamental existence condition, referred to as the Global Exothermic Condition (GEC), of the mechanical-thermal equilibrium model is provided. The aforementioned reference shows the necessity of paying special attention to the equations of state and their adjustment. The careful selection of the thermodynamic parameters for the EOSs of the reactant and the detonation products serves to forestall a pathological detonation, thereby maintaining a globally exothermic reaction that is consistent with the Zeldovich-von Neumann-Döring (ZND) [18–20] theory.

Another difficulty arises from the equations of state. The use of complex EOSs, such as JWL (Lee et al., 1968 [21]) or CC (Cochran and Chan, 1979 [5]), is inherently challenging. It is important to note that these EOSs are not general in the sense that their range of validity is restricted. However, in a numerical simulation, all thermodynamic states can appear, including those with very high pressure at the von Neumann spike and pressure close to zero after gas expansion, as well as those with very high or very low temperature. Extreme values emerge when the range of validity is exceeded, leading to a phenomenon known as “loss of convexity” of the formulation, wherein the speed of sound is no longer defined, the

temperature becomes negative, the thermal expansion and isothermal compressibility coefficients become negative, and the simulation ultimately fails. Indeed, the convexity of the equation of state implies the positivity of the squared speed of sound, the positivity of the temperature, and the positivity of the thermal expansion and isothermal compressibility coefficients. Convexity is essential as it describes a thermodynamically stable equation of state (Menikoff, 2015 [22]). When the equation of state is used outside its domain of validity, issues related to convexity emerge. Details about convexity and various forms of convexity expressions are available in the study by Godunov et al. (1979) [23], Menikoff and Plohr (1989) [24], Chiapolino and Saurel (2018) [25], and Neron and Saurel (2022) [26].

The present paper proposes to address these shortcomings by adopting a novel approach to the thermodynamic aspects. The JWL and CC EOSs, along with other formulations, are limited in their range of validity. The reason for this is that their fit is based on a reference curve in the (p, v) plane (p and v being, respectively, the pressure and specific volume). When the thermodynamic state deviates significantly from the reference curve, the validity of the thermodynamic state is compromised. Numerical simulations frequently fail as a result of this defect. The scientific community has been grappling with this challenge for decades. One approach is to extend the equation of state with expressions that maintain the squared speed of sound as a positive quantity. However, this extension method is not without limitations and involves a degree of arbitrariness. The literature on this subject is scarce, and the long-term viability of extension methods remains uncertain.

In a recent publication, Neron et al. (2023) [27] have put forth a methodology that markedly addresses these shortcomings. The method is founded upon two equations of state. A predictor equation of state (PEOS), which is much simpler and is convex over a wide range of pressure and density, and a target equation of state (TEOS), which is in fact the physical equation of state (*e.g.*, JWL or CC), are employed. At each time step of the numerical method, which encompasses processes such as the Riemann solver and pressure relaxation, the predictor equation of state is employed. However, to maintain computation validity, it is necessary to calculate the parameters of the equation of state in a manner that satisfies a number of compatibility conditions. These conditions are ensured by a method referred to as "thermodynamic relaxation", which is employed after each time step. The two equations of state, "predictor" and "target", are thus rendered perfectly compatible at every time step of the computation, with the exception of the time step during which the simulation is conducted with the "predictor" equation of state. This approach offers several advantages:

- Simulations are faster. The observed gain ranges from a factor of 2 to 10, depending on the conditions and the number of materials under consideration (Neron et al., 2023 [27]).
- Robustness is significantly improved. Indeed, in the event that the thermodynamic state falls outside the range of validity of the target or real equation of state, the simulation continues with the last parameters of the predictor equation of state, which are transported with the flow. Neron et al. (2023) [27] have demonstrated that the solutions obtained are valid with this "automatic" extension.
- The extension of the "target" equation of state is automatic in the sense that, when the convexity criteria are no longer satisfied, the "predictor" equation of state continues the computations with the last parameters calculated from those of the "target" equation of state.

The goal of the present paper is to extend the thermodynamic relaxation method to pressure-and-temperature equilibrium multiphase mixtures to address detonations of condensed explosives under the assumption of pressure and temperature equilibrium among the phases. This goal is achieved within the framework of the diffuse interface model proposed by

Saurel et al. (2009) [28], with the objective of facilitating both temperature-pressure thermodynamic computations and the management of material interfaces. Indeed, condensed explosives are always confined by a surrounding material, and the dynamics of the detonation is linked to the motion of the interface.

The paper is organized as follows. The target and predictor equations of state are presented in Sections 2 and 3, respectively. The flow model is introduced in Section 4. In order to determine the thermodynamic state that corresponds to the specified TEOS, the flow model is modified and additional equations are introduced for each of the thermodynamic parameters of PEOS. The pressure relaxation process is introduced in Section 5. These sections present an abridged version of the original publication by Neron et al. (2023) [27], providing a summary of the essential elements required to extend the method to mechanical and thermal equilibrium. The following sections will address the topic of mechanical and thermal equilibrium, which represents the central focus of this paper. Section 6 is dedicated to the introduction of temperature relaxation source terms. The extension of the thermodynamic relaxation method, in order to encompass both mechanical and thermal equilibrium, is subsequently addressed in Section 7. A summary of the proposed method is provided in the same section. Numerical examples of flows evolving in mechanical and in mechanical-thermal equilibrium are presented in Section 8. They show that the thermodynamic relaxation method enables the solution to be computed in a significantly more efficient manner. In Section 9, mass transfer source terms are introduced and enable the treatment of detonation waves in condensed explosives. Finally, Section 10 presents 1D and 2D detonation test cases to illustrate the benefits of the present method. Conclusions are drawn in Section 11.

2. Target EOS (TEOS)

The target equation of state (TEOS) is the equation of state that is targeted by the thermodynamic relaxation method (Neron et al., 2023 [27]). While TEOS in the present context is of the Mie-Grüneisen (MG) form, this is not a limitation.

2.1 Mie-Grüneisen EOS for a single material

The Mie-Grüneisen EOS is a versatile and accurate formulation that is widely used in the field of detonations with condensed energetic materials. The commonly used functions of the MG EOS read for a material k as

$$\begin{cases} p_k\left(v_k, e_k\right) = \dfrac{\Gamma_k}{v_k}\left(e_k - e_{k,\mathrm{EOS}}\left(v_k\right)\right) + p_{k,\mathrm{EOS}}\left(v_k\right), \\ p_k\left(v_k, T_k\right) = \dfrac{\Gamma_k C_{v,k} T_k}{v_k} + p_{k,\mathrm{EOS}}\left(v_k\right), \\ e_k\left(v_k, T_k\right) = C_{v,k} T_k + e_{k,\mathrm{EOS}}\left(v_k\right), \\ c_k^2\left(p_k, v_k\right) = v_k\left(\Gamma_k + 1\right)\left(p_k - p_{k,\mathrm{EOS}}\left(v_k\right)\right) - v_k^2 \dfrac{\mathrm{d}p_{k,\mathrm{EOS}}\left(v_k\right)}{\mathrm{d}v_k}. \end{cases} \tag{2.1}$$

The notations are conventional in the two-phase flow literature. The variables p_k, v_k, e_k, T_k, and c_k represent the pressure, the specific volume, the specific internal energy, the temperature, and the sound speed, respectively. The parameters Γ_k and $C_{v,k}$ represent the Grüneisen coefficient and the specific heat at constant volume respectively. The heat capacity is considered a constant parameter in this paper. The Grüneisen coefficient is also a constant, except for the Noble-Abel-stiffened-gas (NASG) EOS as will be seen later. Functions $p_{k,\mathrm{EOS}}\left(v_k\right)$ and $e_{k,\mathrm{EOS}}\left(v_k\right)$ are specific to the MG-type EOS under consideration. Such equations of state include the Cochran-Chan (CC) EOS [5], widely used to model the thermodynamics of the condensed phase, and the JWL EOS [21], widely used to model the thermodynamics of the detonation products.

The CC and JWL equations of state are presented in Appendix A and Appendix B along with the various parameters used in this paper. MG-type equations of state (2.1) present at least three difficulties:

- Both the domain of physical validity and the domain of convexity are restricted;
- Consequently, the robustness of the computations is challenging. This is especially true in the zones of vanishing phases, which often occur in a multiphase computation;
- The density $\rho_k = 1/v_k$ is not explicit and must be computed using an iterative method, such as Newton-Raphson's. The reason for this is the nonlinear dependence of the $p_{k,\text{EOS}}(v_k)$ and $e_{k,\text{EOS}}(v_k)$ functions on the specific volume. Robustness problems then reappear, in addition to excessive computational time associated with the required iterative process. The pressure relaxation solver requires the density as a function of pressure.

These elements prompted the authors to develop an innovative and efficient thermodynamic relaxation method to address the three difficulties mentioned above. This novel method is fully presented in Neron et al. (2023) [27] in the context of temperature disequilibrium. The main ideas are summarized in Sections 3-4-5, and the method is then extended to mechanical and thermal equilibrium in Sections 6-7.

3. Predictor EOS (PEOS)

The predictor EOS (PEOS) refers to the simplified thermodynamic model that aims to recover the thermodynamic state of the target model, at least locally at a given thermodynamic point. The Noble-Abel-stiffened-gas (NASG) equation of state is a combination of simplicity and richness from a physical point of view (Le Métayer and Saurel, 2016 [29]),

$$\begin{cases} p_k(v_k, e_k) = \dfrac{(\gamma_k^* - 1)\left(e_k - e_{k,\text{ref}}^*\right)}{v_k - b_k^*} - \gamma_k^* p_{\infty,k}^*, = \dfrac{R_k^*\left(e_k - e_{k,\text{ref}}^*\right)}{C_{v,k}^*(v_k - b_k^*)} - \left(\dfrac{R_k^*}{C_{v,k}^*} + 1\right) p_{\infty,k}^*, \\ p(v_k, T_k) = \dfrac{(\gamma_k^* - 1) C_{v,k}^* T_k}{v_k - b_k^*} - p_{\infty,k}^* = \dfrac{R_k^* T_k}{v_k - b_k^*} - p_{\infty,k}^*, \\ e_k(v_k, T_k) = C_{v,k}^* T_k + p_{\infty,k}^*(v_k - b_k^*) + e_{k,\text{ref}}^*, \\ c_k^2(p_k, v_k) = \dfrac{\gamma_k^* v_k^2\left(p_k + p_{\infty,k}^*\right)}{v_k - b_k^*} = \dfrac{v_k^2\left(R_k^* + C_{v,k}^*\right)\left(p_k + p_{\infty,k}^*\right)}{C_{v,k}^*(v_k - b_k^*)}. \end{cases} \tag{3.1}$$

The NASG equation of state has the following nice properties:

- It is fully explicit;
- It encompasses the three fundamental molecular forces observed in matter: agitation, short-range repulsion, and long-range attraction in a simple formulation;
- It is convex convex over a wide range of pressures: $p_k > -p_{\infty,k}^*$.

Furthermore, the NASG EOS can be expressed in the MG form (2.1) through the use of the following functions:

$$\begin{cases} \Gamma_k^* = \Gamma_k^*(v_k) & = v_k \left.\dfrac{\partial p_k}{\partial e_k}\right|_{v_k} = \dfrac{\gamma_k^* - 1}{1 - \rho_k b_k^*}, \\ e_{k,\text{EOS}}(v_k) & = e_{k,\text{NASG}}(v_k) = p_{\infty,k}^*(v_k - b_k^*) + e_{k,\text{ref}}^*, \\ p_{k,\text{EOS}}(v_k) & = p_{k,\text{NASG}} = -p_{\infty,k}^*. \end{cases} \tag{3.2}$$

The Grüneisen coefficient depends on the density (or specific volume) for the NASG EOS. The parameter b_k^* represents the covolume and serves to model short-range repulsive effects. The parameter $p_{\infty,k}^*$ represents attractive forces that are present only in condensed matter. The term $e_{k,\text{ref}}$ denotes the reference (or formation) energy. Finally, $\gamma_k^* = C_{p,k}^*/C_{v,k}^* = R_k^*/C_{v,k}^* + 1$ is the adiabatic coefficient associated with thermal agitation. In this last relation, $C_{p,k}^*$ and $C_{v,k}^*$ denote the heat capacity at constant pressure and constant volume respectively, and R_k^* is the specific gas constant. Attractive and repulsive effects are assumed to be constant in this representation, making the NASG EOS a simple formulation. Furthermore, it simply reduces to the ideal-gas EOS when $b_k^* = 0$ and $p_{\infty,k}^* = 0$ are set. Details on the NASG EOS can be found in Le Métayer and Saurel (2016) [29] and Chiapolino and Saurel (2018) [25].

As in the original publication (Neron et al., 2023 [27]), superscript * has been added to specify the parameters that are to be adapted in order to match the TEOS formulation. The thermodynamic relaxation method uses the NASG EOS (3.1) as a predictor and as a closure to the flow model. The flow model is then modified accordingly and is presented in the following section.

4. Hyperbolic formulation with relaxation

The system of Saurel et al. (2009) [28] is a homo-kinetic model considering pressure and temperature disequilibrium. It does consist of a hyperbolic overdetermined system composed of the following equations,

$$\begin{cases} \dfrac{\partial \alpha_k}{\partial t} + \mathbf{u}\cdot grad\,(\alpha_k) = \mu(p_k - p_l) \quad \text{with} \quad \mu \to +\infty, \\ \dfrac{\partial\,(\alpha_k\rho_k)}{\partial t} + div\,(\alpha_k\rho_k\mathbf{u}) = 0, \\ \dfrac{\partial\,(\rho\mathbf{u})}{\partial t} + div\left(\rho\mathbf{u}\otimes\mathbf{u} + p\underline{\underline{\mathbf{I}}}\right) = 0, \\ \dfrac{\partial\,(\alpha_k\rho_k e_k)}{\partial t} + div\,(\alpha_k\rho_k e_k\mathbf{u}) + \alpha_k p_k\, div\,(\mathbf{u}) = -\mu p_I(p_k - p_l) + \vartheta_{k,l}\,(T_k - T_l)\,, \\ \dfrac{\partial\,(\rho E)}{\partial t} + div\left(\left[\rho E + p\right]\mathbf{u}\right) = 0. \end{cases} \tag{4.1}$$

A frame of reference $\mathbf{X} = (x, y, z)$ is chosen and the time variable is denoted by t. The mathematical notations are as follows: div is the divergence operator, $grad$ is the gradient operator, $\otimes$ is the tensor product, and $\underline{\underline{\mathbf{I}}}$ is the unit tensor. The variables ρ_k, p_k, T_k, and e_k denote the density, pressure, temperature, and internal energy of phase k respectively. The volume fraction of phase k is denoted by α_k. Index l denotes the conjugate phase to k, *i.e.*, $k = 1$ implies $l = 2$ and vice versa. The mixture internal energy is defined as $e = \sum Y_k e_k$ where $Y_k = \alpha_k\rho_k/\rho$ denotes the mass fraction of phase k. The mixture density and pressure are defined as $\rho = \sum \alpha_k\rho_k$ and $p = \sum \alpha_k p_k$, respectively. Finally, the mixture total energy reads $E = e + \frac{1}{2}(\mathbf{u}\cdot\mathbf{u})$ where $\mathbf{u}$ is the mixture velocity vector and $\cdot$ is the dot product.

The parameter μ controls the rate at which pressure equilibrium is reached. As the present model intends to recover the solution to the mechanical equilibrium model of Kapila et al. (2001) [1], stiff pressure relaxation is considered: $\mu \to +\infty$. Similarly, the parameter $\vartheta_{k,l}$ represents the rate at which temperature equilibrium is reached between materials k and l. The inert materials evolve only in mechanical equilibrium, so $\vartheta_{k,l} = 0$. It is, however, assumed that the reactant (R) and detonation products (DP) evolve in mechanical and thermal equilibrium. Stiff temperature equilibrium is then addressed through $\vartheta_{k,l} \to +\infty$ with $k = \text{DP}$ and $l = \text{R}$, as will be seen later (Section 6). Mass source terms are currently omitted for the sake clarity. Section 9 will be devoted to the introduction of mass transfer terms.

The interfacial pressure appearing on the right-hand side reads $p_I = \frac{\sum \frac{p_k}{Z_k}}{\sum \frac{1}{Z_k}}$, where $Z_k = \rho_k c_k$ is the acoustic impedance. The x-split one-dimensional formulation is hyperbolic with wave speeds u and $u \pm c_f$ with the following definition for the squared sound speed: $c_f^2 = \sum Y_k c_k^2$. System (4.1) of Saurel et al. (2009) [28] is capable of addressing material interfaces, as it is able to match the interface conditions of equal pressures and velocities (see Saurel et al., 2009 [28], Chiapolino et al., 2017 [30], Saurel and Pantano, 2018 [31] to cite a few). This flow model is of particular interest in the present detonation context as it is capable of addressing two-phase mixtures in mechanical equilibrium as well as in mechanical-and-thermal equilibrium through relaxation source terms, as will be seen further in Sections 5, 6, and 9.

4.1 Extended flow model and thermodynamic relaxation

As mentioned earlier, System (4.1) is augmented by transport-relaxation equations for each phase k using the predictor equation of state (PEOS). These are expressed in conservative form with the help of the mixture mass equation,

$$\begin{cases} \dfrac{\partial \left(\rho b_k^*\right)}{\partial t} + div\left(\rho b_k^* \mathbf{u}\right) = \dfrac{\rho}{\tau}\left(b_k\left(v_k, e_k\right) - b_k^*\right), \\ \dfrac{\partial \left(\rho p_{\infty,k}^*\right)}{\partial t} + div\left(\rho p_{\infty,k}^* \mathbf{u}\right) = \dfrac{\rho}{\tau}\left(p_{\infty,k}\left(v_k, e_k\right) - p_{\infty,k}^*\right), \\ \dfrac{\partial \left(\rho R_k^*\right)}{\partial t} + div\left(\rho R_k^* \mathbf{u}\right) = \dfrac{\rho}{\tau}\left(R_k\left(v_k, e_k\right) - R_k^*\right), \\ \dfrac{\partial \left(\rho C_{v,k}^*\right)}{\partial t} + div\left(\rho C_{v,k}^* \mathbf{u}\right) = \dfrac{\rho}{\tau}\left(C_{v,k}\left(v_k, e_k\right) - C_{v,k}^*\right), \\ \dfrac{\partial \left(\rho e_{k,\mathrm{ref}}^*\right)}{\partial t} + div\left(\rho e_{k,\mathrm{ref}}^* \mathbf{u}\right) = \dfrac{\rho}{\tau}\left(e_{k,\mathrm{ref}}\left(v_k, e_k\right) - e_{k,\mathrm{ref}}^*\right), \\ \text{with } \tau \to 0^+ \text{ when the convexity relations (see Section 4.2) are fulfilled, otherwise } \tau \to +\infty. \end{cases} \tag{4.2}$$

As fully detailed in Neron et al. (2023) [27], System (4.1)-(4.2) forms the extended flow model with the transport-relaxation equations, which demonstrates enhanced efficiency in numerical resolution. Indeed, from a computational standpoint, this approach is more convenient, faster, and the prolongation outside the range of convexity is automatic, thereby maintaining the hyperbolic nature of the formulation. In contrast, the conventional two-phase model (4.1) with TEOS loses this property when convexity conditions are violated. The hyperbolic equations, describing conservation laws, become ill-posed.

As argued in Neron et al. (2023) [27], for the predictions with the NASG EOS (PEOS) to be valid, it is necessary to calculate the parameters of the equation of state in a way that satisfies a number of compatibility conditions. These conditions are as follows:

$$\begin{cases} T_{k,\mathrm{PEOS}}\left(v_k, e_k\right) = T_{k,\mathrm{TEOS}}\left(v_k, e_k\right), \\ p_{k,\mathrm{PEOS}}\left(v_k, e_k\right) = p_{k,\mathrm{TEOS}}\left(v_k, e_k\right), \\ c_{k,\mathrm{PEOS}}^2\left(v_k, e_k\right) = c_{k,\mathrm{TEOS}}^2\left(v_k, e_k\right). \end{cases} \tag{4.3}$$

This choice is motivated by both numerical and physical reasons. The specific volume v_k and internal energy e_k are part of the conservative variables and are provided by the numerical resolution of the flow model (System (4.1)), regardless of the equation of state (PEOS or TEOS). The pressure p_k and temperature T_k are among the primitive variables. In both the PEOS and TEOS, these primitive variables are equated, as is the sound speed c_k. As System (4.1)-(4.2) is a non-equilibrium flow model, the sub-characteristic condition of Liu (1987) [32] must be satisfied when PEOS is used instead of TEOS. Here it corresponds to: $c_{k,\mathrm{PEOS}}^2\left(v_k, e_k\right) \geq c_{k,\mathrm{TEOS}}^2\left(v_k, e_k\right)$, which is fulfilled by the last relation of (4.3). However,

System (4.1)-(4.2), corresponding to the extended model, includes all five NASG parameters $b_k^*(v_k, e_k)$, $p_{\infty,k}^*(v_k, e_k)$, $R_k^*(v_k, e_k)$, $C_{v,k}^*(v_k, e_k)$, and $e_{k,\text{ref}}^*(v_k, e_k)$, while only three compatibility conditions are provided at this point. It is then necessary either to include some additional compatibility conditions or to remove some NASG parameters.

Covolume effects are absent in the MG formulation (2.1). It motivates $b_k^* = 0$ in the various phases. The first equation of (4.2) is then removed. The predictor equation of state (PEOS) is then reduced to the stiffened-gas (SG) equation of state. From a numerical standpoint, the SG EOS is beneficial, as it is algebraically simple, facilitates the construction of exact Riemann solvers (Godunov et al., 1976 [33], Plohr, 1988 [34]), and is consistent with physical contact discontinuities, as detailed in Saurel and Abgrall (1999) [35]. However, for the sake of generality, the term NASG will be used throughout the remainder of the paper to refer to the PEOS EOS. In addition, the same Grüneisen coefficient is used in both PEOS and TEOS: $\Gamma_k^* = \Gamma_k$. The Grüneisen parameter quantifies the relation between the thermal and elastic properties of a material [36]. It can be interpreted as the variation of pressure with thermal energy per unit volume of a material held at a constant volume [37, 38]. As a result of $\Gamma_k^* = \Gamma_k$, the thermodynamic parameters R_k^* and $C_{v,k}^*$ are linked through Mayer's relation as detailed in Appendix A of Neron et al. (2023) [27]: $C_{v,k}^* = \frac{R_k^*}{\Gamma_k}$. The fourth equation of (4.2) is then removed as well.

Consequently, only 3 coefficients remain to be determined: $R_k^*(v_k, e_k)$, $p_{\infty,k}^*(v_k, e_k)$, and $e_{k,\text{ref}}^*(v_k, e_k)$. These coefficients are determined to satisfy the three conditions (4.3). Further details can be found in Neron et al. (2023) [27]. Using the PEOS equations (3.1), the solution to System (4.3) is as follows,

$$\begin{cases} R_k^*(v_k, e_k) = \dfrac{c_{k,\text{TEOS}}^2(v_k, e_k)}{(\Gamma_k + 1)\, T_{k,\text{TEOS}}(v_k, e_k)}, \\ p_{\infty,k}^*(v_k, e_k) = \dfrac{c_{k,\text{TEOS}}^2(v_k, e_k)}{v_k(\Gamma_k + 1)} - p_{k,\text{TEOS}}(v_k, e_k), \\ e_{k,\text{ref}}^*(v_k, e_k) = e_k - \dfrac{c_{k,\text{TEOS}}^2(v_k, e_k)}{\Gamma_k} + v_k p_{k,\text{TEOS}}(v_k, e_k). \end{cases} \tag{4.4}$$

Relations (4.4) are used to reset the three thermodynamic parameters $R_k^*(v_k, e_k)$, $p_{\infty,k}^*(v_k, e_k)$, and $e_{k,\text{ref}}^*(v_k, e_k)$ before the next time step, *i.e.*, before the next hyperbolic-transport step.

4.2 Relaxation switch

Relations (4.3) and (4.4) make the predictor EOS and the target EOS compatible. They consist of the first fundamental element of the thermodynamic relaxation method developed by Neron et al. (2023) [27]. When the thermodynamic relaxation step (4.4) is achieved, asymptotic considerations show that the flow model with PEOS tends to the solution of TEOS. A second fundamental element complements the method. It consists of the so-called relaxation switch. In fact, TEOS is sometimes inappropriate in the sense that its domain of validity is limited and issues related to convexity appear. These issues have dramatic consequences on the computed thermodynamic state. In such cases, the target EOS is no longer physical and cannot be used as such.

Using the method described by Neron et al. (2023) [27] and Chiapolino et al. (2024) [4], the following convexity criteria

are derived for the MG EOS (2.1),

$$\begin{cases} p_k > p_{k,\mathrm{EOS}}\left(v_k\right) + \dfrac{v_k}{\Gamma_k + 1}\dfrac{\mathrm{d}p_{k,\mathrm{EOS}}\left(v_k\right)}{\mathrm{d}v_k}, \\ p_k > p_{k,\mathrm{EOS}}\left(v_k\right), \\ p_k > p_{k,\mathrm{EOS}}\left(v_k\right) + v_k\dfrac{\mathrm{d}p_{k,\mathrm{EOS}}\left(v_k\right)}{\mathrm{d}v_k}. \end{cases} \tag{4.5}$$

These three relations imply the positivity of the squared speed of sound, the positivity of the temperature, and the positivity of the thermal expansion and isothermal compressibility coefficients respectively. With the present method, if the convexity criteria (4.5) are violated, the thermodynamic reset is switched off and the computations continue with the last PEOS parameters. These parameters are still transported by the flow but are not relaxed to the non-convex TEOS state. This means that the relaxation time in (4.2) no longer tends to zero: $\tau \to 0^+$, but now tends to infinity: $\tau \to +\infty$. Since the convexity domain of the PEOS (NASG) is much larger, the computations become very robust. This method automatically extends the MG EOS and guarantees the continuity of all thermodynamic variables. At this point, the thermodynamic relaxation method developed by Neron et al. (2023) [27] is recovered. The reader is referred to this reference for further details. The relaxation processes involved in the present two-phase flow model (4.1)-(4.2) are addressed in the following.

5. Stiff pressure relaxation

The phases (materials) as described by System (4.1) are in pressure disequilibrium. Upon completion of the pressure relaxation process (Le Métayer et al., 2013 [39]), the phases reach a common pressure (the temperatures being different at this point). Details of the pressure relaxation process are provided in Neron et al. (2023) [27] in the context of both TEOS and PEOS. The simplicity and efficiency of the present thermodynamic relaxation method is demonstrated. In fact, TEOS requires two nested Newton loops for pressure relaxation, which significantly affects robustness and computational cost time, while PEOS requires only one loop. Furthermore, in the specific case where only two materials are present, such as the reactant and the detonation products, an explicit solution appears. The reader is referred to Neron et al. (2023) [27] for details on the stiff pressure relaxation process.

The following section addresses the process of temperature relaxation, as the purpose of this paper is to extend the thermodynamic relaxation method to address condensed explosives under the assumption of pressure and temperature equilibrium between the phases. The remainder of the paper constitutes the core contribution of this study.

6. Thermal equilibrium

As mentioned in the Introduction, most engineering computations dealing with condensed energetic materials use the reactive Euler equations with a mixture equation of state based on temperature and pressure equilibrium among the phases. This model assumes that the reactant and the detonation products evolve in pressure and temperature equilibrium. As a consequence of this assumption, the reactive Euler equations are not suited to address material interfaces. However as a condensed explosive is invariably confined by external materials, the treatment of material interfaces is essential. For this reason, the non-equilibrium model (4.1) of Saurel et al. (2009) [28] is used with a stiff pressure relaxation procedure (Section 5) to compute the solution to the mechanical equilibrium model due to Kapila et al. (2001) [1]. It is now necessary

to compute mechanical and thermal equilibrium between two specific materials. This will be achieved via an additional relaxation process that takes into account the temperatures.

6.1 Stiff temperature relaxation

In the absence of convective fluxes and pressure relaxation source terms, System (4.1) reads:

$$\begin{cases} \dfrac{\partial \alpha_k}{\partial t} = 0, \\ \dfrac{\partial \left(\alpha_k \rho_k\right)}{\partial t} = 0, \\ \dfrac{\partial \left(\rho \mathbf{u}\right)}{\partial t} = 0, \\ \dfrac{\partial \left(\alpha_k \rho_k e_k\right)}{\partial t} = \vartheta_{k,l} \left(T_k - T_l\right), \\ \dfrac{\partial \left(\rho E\right)}{\partial t} = 0. \end{cases} \tag{6.1}$$

The parameter $\vartheta_{k,l}$ represents the rate at which temperature equilibrium is reached between materials k and l. The inert materials evolve only in mechanical equilibrium, so $\vartheta_{k,l} = 0$. It is, however, assumed that the reactant (R) and detonation products (DP) evolve in mechanical and thermal equilibrium. Stiff temperature relaxation is then addressed through $\vartheta_{k,l} \to +\infty$ with $k = \text{DP}$ and $l = \text{R}$.

System (6.1) reveals that the volume fractions α_k and apparent masses $\alpha_k \rho_k$ remain constant during the temperature relaxation process. Consequently, the mixture density ρ, the densities of the materials ρ_k, as well as the mass fractions Y_k also remain unchanged. Additionally, the third and fifth relations of (6.1) reveal that the mixture velocity $\mathbf{u}$ and mixture total energy E are constant. The mixture internal energy e is consequently unchanged and only the internal energies of the materials e_k are modified through the temperature relaxation process.

As the mixture internal energy e is unchanged during the process, it reads:

$$e = Y_{\text{R}} e_{\text{R}} \left(v_{\text{R}}, T^{(1)}\right) + Y_{\text{DP}} e_{\text{DP}} \left(v_{\text{DP}}, T^{(1)}\right) + \sum_{k \neq \text{R,DP}} Y_k e_k. \tag{6.2}$$

In Relation (6.2), $T^{(1)}$ denotes the relaxed temperature, corresponding to the temperature of the mixture made of the reactant (R) and the detonation products (DP). In the present contribution, MG-type equations of state (2.1) are used, either for the target EOS or the predictor EOS. As the NASG predictor EOS can be expressed in the generic MG form through Relation (3.2), the subsequent derivations thus apply to both the TEOS and PEOS. Under the MG form, the internal energy of a material k reads:

$$e_k \left(v_k, T_k\right) = C_{v,k} T_k + e_{k,\text{EOS}} \left(v_k\right). \tag{6.3}$$

The combination of Eq. (6.2) and Eq. (6.3) yields an explicit formulation of the relaxed temperature:

$$T^{(1)} \left(v_k, e\right) = \frac{e - \left(Y_{\text{DP}} e_{\text{DP,EOS}} \left(v_{\text{DP}}\right) + Y_{\text{R}} e_{\text{R,EOS}} \left(v_{\text{R}}\right)\right) - \sum_{k \neq \text{R,DP}} Y_k e_k}{Y_{\text{DP}} C_{v,\text{DP}} + Y_{\text{R}} C_{v,\text{R}}}. \tag{6.4}$$

Upon computation of the relaxed temperature $T^{(1)} \left(v_k, e\right)$, the internal energies are updated using their own equation of state: $e_k = e_k \left(v_k, T^{(1)}\right)$, either with PEOS or TEOS. Note that in the event where thermal equilibrium is considered

between all materials, Relation (6.4) transforms to:

$$T^{(1)}\left(v_k, e\right) = \frac{e - \sum Y_k e_{k,\mathrm{EOS}}\left(v_k\right)}{\sum Y_k C_{v,k}}. \tag{6.5}$$

The consecutive pressure and temperature relaxation processes allow to recover the solution to the multi-component Euler equations, which involve mechanical and thermal equilibrium. Mass transfer can be incorporated between the two relaxation processes, as will be seen in Section 9. The various relaxation processes involve the equations of state of the materials. As mentioned in the Introduction, the use of complex EOSs, such as JWL or CC, is inherently challenging. Such equations of state have a restricted validity range, a restricted convexity range, and the expression of the density is not explicit leading to time-consuming computations.

Consequently, the various relaxation processes are achieved with the NASG predictor equation of state (PEOS). The NASG equation of state is much simpler than general Mie-Grüneisen type EOSs. As a result, computations are markedly faster. Furthermore, the NASG EOS involves a much larger range of convexity that significantly improves the robustness of computations. Nevertheless, for the NASG predictions to be valid, the associated parameters must be determined to meet compatibility conditions. These conditions are ensured by what is referred to as the thermodynamic relaxation (Neron et al, 2023 [27]). In order to take into account thermal equilibrium, it is necessary to extend the thermodynamic relaxation method, particularly with regard to the computation of the PEOS parameters.

7. Extension of the thermodynamic relaxation to address mechanical and thermal equilibrium

The thermodynamic relaxation method, which was initially developed by Neron et al. (2023) [27] and is presented in Section 4.1, is designed to address single-phase and diffuse interface models. However, in the present context, the situation is different, as some materials evolve in mechanical and thermal equilibrium. The situation then involves a mixture of materials and demands a reconsideration of the target equation of state: TEOS. The computation of the PEOS parameters remains founded on the equality of pressures, temperatures, and squared sound speeds between TEOS and PEOS [27]. Therefore, the fundamental principles of the relaxation method remain unchanged, but the target equation of state, which is in fact the physical equation of state, becomes **the equation of state of the mixture evolving in mechanical and thermal equilibrium**.

The target temperature $T_{k,\mathrm{TEOS}}$, thus, becomes the mixture temperature that is given by Eq. (6.4) or (6.5). This temperature depends upon the specific volumes of the material v_k and the mixture internal energy e, in contrast to the original thermodynamic relaxation where the target equation of state is determined using both v_k and e_k. The target pressure $p_{k,\mathrm{TEOS}}$ shall be determined through the mixture internal energy e as well. Consequently, $p_{k,\mathrm{TEOS}}$ is computed as either $p_{k,\mathrm{TEOS}}\left(v_k, T_{k,\mathrm{TEOS}}\right)$ or $p_{k,\mathrm{TEOS}}\left(v_k, e_k^{**}\right)$ where $e_k^{**} = e_{k,\mathrm{TEOS}}\left(v_k, T_{k,\mathrm{TEOS}}\right)$ is updated by the target thermal equation state (6.3). Similarly, the target squared speed of sound $c^2_{k,\mathrm{TEOS}}$ is also computed as either $c^2_{k,\mathrm{TEOS}}\left(v_k, T_{k,\mathrm{TEOS}}\right)$

or $c^2_{k,\text{TEOS}}\left(v_k, e^{**}_k\right)$ with $e^{**}_k = e_{k,\text{TEOS}}\left(v_k, T_{k,\text{TEOS}}\right)$. The three compatibility relations (4.3) become:

$$\begin{cases} T_{k,\text{PEOS}}\left(v_k, e\right) = T_{k,\text{TEOS}}\left(v_k, e\right) = \dfrac{e - \left(Y_{\text{DP}} e_{\text{DP,EOS}}\left(v_{\text{DP}}\right) + Y_{\text{R}} e_{\text{R,EOS}}\left(v_{\text{R}}\right)\right) - \sum_{k \neq \text{R,DP}} Y_k e_k}{Y_{\text{DP}} C_{v,\text{DP}} + Y_{\text{R}} C_{v,\text{R}}}, \\ p_{k,\text{PEOS}}\left(v_k, e\right) = p_{k,\text{TEOS}}\left(v_k, T_{k,\text{TEOS}}\left(v_k, e\right)\right) = p_{k,\text{TEOS}}\left(v_k, e^{**}_k\right), \\ c^2_{k,\text{PEOS}}\left(v_k, e\right) = c^2_{k,\text{TEOS}}\left(v_k, T_{k,\text{TEOS}}\left(v_k, e\right)\right) = c^2_{k,\text{TEOS}}\left(v_k, e^{**}_k\right), \\ \text{with } \; e^{**}_k = e_{k,\text{TEOS}}\left(v_k, T_{k,\text{TEOS}}\left(v_k, e\right)\right) = C_{v,k} T_{k,\text{TEOS}}\left(v_k, e\right) + e_{k,\text{EOS}}\left(v_k\right). \end{cases} \tag{7.1}$$

The following section provides a summary of the overall thermodynamic relaxation method.

7.1 Summary of the thermodynamic relaxation method

The thermodynamic relaxation method is founded upon two equations of state: a predictor equation of state (PEOS), which is much simpler and is convex over a wide range of pressure and density, and a target equation of state (TEOS), which is, in fact, the physical equation of state (*e.g.*, JWL or CC). At each time step of the numerical method, which encompasses processes such as the Riemann solver and pressure-temperature relaxation and mass transfer, the predictor equation of state is employed, yielding a faster and more efficient computational method. However, for the computations to be valid, it is necessary to calculate the parameters of the equation of state in a manner that satisfies a number of compatibility conditions. These conditions are ensured by the so called "thermodynamic relaxation" method, which is employed after each time step. The two equations of state, "predictor" and "target", are thus rendered perfectly compatible at every time step of the computation, with the exception of the time step during which the simulation is conducted with the "predictor" equation of state. The associated sequence is used:

- Initialization of two thermodynamic variables such as (p_k, ρ_k) or (p_k, T_k) and computation of the third variable such as T_k or ρ_k with TEOS (2.1). The initial internal energies e_k are computed with TEOS as well. Thereafter, the PEOS parameters are computed with Relations (4.4) and either Eq. (2.1) or Relations (7.1) as the target EOS depending on the desired equilibrium (mechanical or mechanical-thermal). The TEOS and PEOS are initially merged in terms of p_k, T_k, and c_k (Relations (4.3)).

- Resolution of the hyperbolic step with PEOS (3.1). This step consists of the resolution of the two-phase flow system (4.1)-(4.2) without source terms.

- Stiff pressure relaxation with PEOS (3.1). The PEOS offers a significant numerical advantage, as it allows for the computation of the relaxed solution with a single iterative method, whereas the TEOS necessitates the use of two embedded iterative methods, as detailed in Neron et al. (2023) [27]. Furthermore, an explicit solution is available with PEOS when only two materials are considered.

- The solution at this point corresponds to that of the mechanical equilibrium model of Kapila et al. (2001) [1]. Mass transfer may be addressed according to the method presented in Section 9. In the case of involvement of a detonation wave, consideration of mass transfer source terms shall involve prior detection of the detonation zone. Details will be provided in Section 9. For both the detonation-zone detection step and the mass transfer step, the PEOS (3.1) is used.

- An additional relaxation process, regarding the temperature of the reactant and the temperature of the detonation products, makes the solution tend to that of the reactive (or multi-component) Euler equations (with or without mass transfer). This temperature relaxation process is achieved with the method presented in Section 6.1 and with PEOS (3.1).

- Thermodynamic relaxation is achieved through Relations (4.4) that are reminded hereafter:

$$\begin{cases} R_k^* = \dfrac{c_{k,\mathrm{TEOS}}^2}{(\Gamma_k+1)\,T_{k,\mathrm{TEOS}}}, \\ p_{\infty,k}^* = \dfrac{c_{k,\mathrm{TEOS}}^2}{v_k\,(\Gamma_k+1)} - p_{k,\mathrm{TEOS}}, \\ e_{k,\mathrm{ref}}^* = e_k^{**} - \dfrac{c_{k,\mathrm{TEOS}}^2}{\Gamma_k} + v_k p_{k,\mathrm{TEOS}}. \end{cases} \tag{7.2}$$

  This relaxation of the PEOS parameters is only achieved if the convexity criteria (4.5) are satisfied with TEOS. These are reminded hereafter:

$$\begin{cases} p_k > p_{k,\mathrm{EOS}}\,(v_k) + \dfrac{v_k}{\Gamma_k+1}\dfrac{\mathrm{d}p_{k,\mathrm{EOS}}\,(v_k)}{\mathrm{d}v_k}, \\ p_k > p_{k,\mathrm{EOS}}\,(v_k)\,, \\ p_k > p_{k,\mathrm{EOS}}\,(v_k) + v_k\dfrac{\mathrm{d}p_{k,\mathrm{EOS}}\,(v_k)}{\mathrm{d}v_k}. \end{cases} \tag{7.3}$$

  In this case, the thermodynamic relaxation is stiff: $\tau \to 0^+$. Conversely, if the convexity criteria are not satisfied, then no relaxation occurs : $\tau \to +\infty$, and consequently, the PEOS parameters are not updated. These have only been transported by the flow, and the next time step will be addressed with a convex equation of state (PEOS). This final step makes the two equations of state, "predictor" and "target", perfectly compatible in the event of a convex TEOS. Regarding TEOS, two situations are possible:

  – The materials evolve in mechanical equilibrium only. In the context of detonation, these materials are inert. In that event, TEOS is given by Relations (2.1) that are used under the following form:

$$\begin{cases} T_{k,\mathrm{TEOS}}\,(v_k,e_k) = \dfrac{e_k - e_{k,\mathrm{EOS}}\,(v_k)}{C_{v,k}}, \\ p_{k,\mathrm{TEOS}}\,(v_k,e_k) = \dfrac{\Gamma_k}{v_k}\,(e_k - e_{k,\mathrm{EOS}}\,(v_k)) + p_{k,\mathrm{EOS}}\,(v_k)\,, \\ c_{k,\mathrm{TEOS}}^2\,(v_k,e_k) = \Gamma_k\,(\Gamma_k+1)\,(e_k - e_{k,\mathrm{EOS}}\,(v_k)) - v_k^2\dfrac{\mathrm{d}p_{k,\mathrm{EOS}}\,(v_k)}{\mathrm{d}v_k}, \\ \text{and } \ e_k^{**} = e_k. \end{cases} \tag{7.4}$$

  – The materials evolve in mechanical and thermal equilibrium. In the context of detonation, these materials are the reactant and the donation products. In that event, TEOS is given by Relations (7.1) that are reminded

hereafter:

$$\begin{cases} T_{k,\mathrm{TEOS}}\left(v_k,e\right)=\dfrac{e-\left(Y_{\mathrm{DP}}e_{\mathrm{DP,EOS}}\left(v_{\mathrm{DP}}\right)+Y_{\mathrm{R}}e_{\mathrm{R,EOS}}\left(v_{\mathrm{R}}\right)\right)-\sum_{k\neq\mathrm{R,DP}}Y_k e_k}{Y_{\mathrm{DP}}C_{v,\mathrm{DP}}+Y_{\mathrm{R}}C_{v,\mathrm{R}}}, \\ p_{k,\mathrm{TEOS}}\left(v_k,T_{k,\mathrm{TEOS}}\left(v_k,e\right)\right)=p_{k,\mathrm{TEOS}}\left(v_k,e_k^{**}\right)=\dfrac{\Gamma_k}{v_k}\left(e_k^{**}-e_{k,\mathrm{EOS}}\left(v_k\right)\right)+p_{k,\mathrm{EOS}}\left(v_k\right), \\ c_{k,\mathrm{TEOS}}^2\left(v_k,T_{k,\mathrm{TEOS}}\left(v_k,e\right)\right)=c_{k,\mathrm{TEOS}}^2\left(v_k,e_k^{**}\right)=\Gamma_k\left(\Gamma_k+1\right)\left(e_k^{**}-e_{k,\mathrm{EOS}}\left(v_k\right)\right)-v_k^2\dfrac{\mathrm{d}p_{k,\mathrm{EOS}}\left(v_k\right)}{\mathrm{d}v_k}, \\ \text{with}\ \ e_k^{**}=e_{k,\mathrm{TEOS}}\left(v_k,T_{k,\mathrm{TEOS}}\left(v_k,e\right)\right)=C_{v,k}T_{k,\mathrm{TEOS}}\left(v_k,e\right)+e_{k,\mathrm{EOS}}\left(v_k\right). \end{cases} \tag{7.5}$$

A simple and convex equation of state (PEOS) is then always used during the entirety of the simulation, with the help of additional transport-relaxation equations. The last step, which is the thermodynamic relaxation step, serves to project the predicted solution onto the target EOS, but only in the event that the target EOS is convex. The overall thermodynamic relaxation method is depicted with the following flowchart (Figure 1).

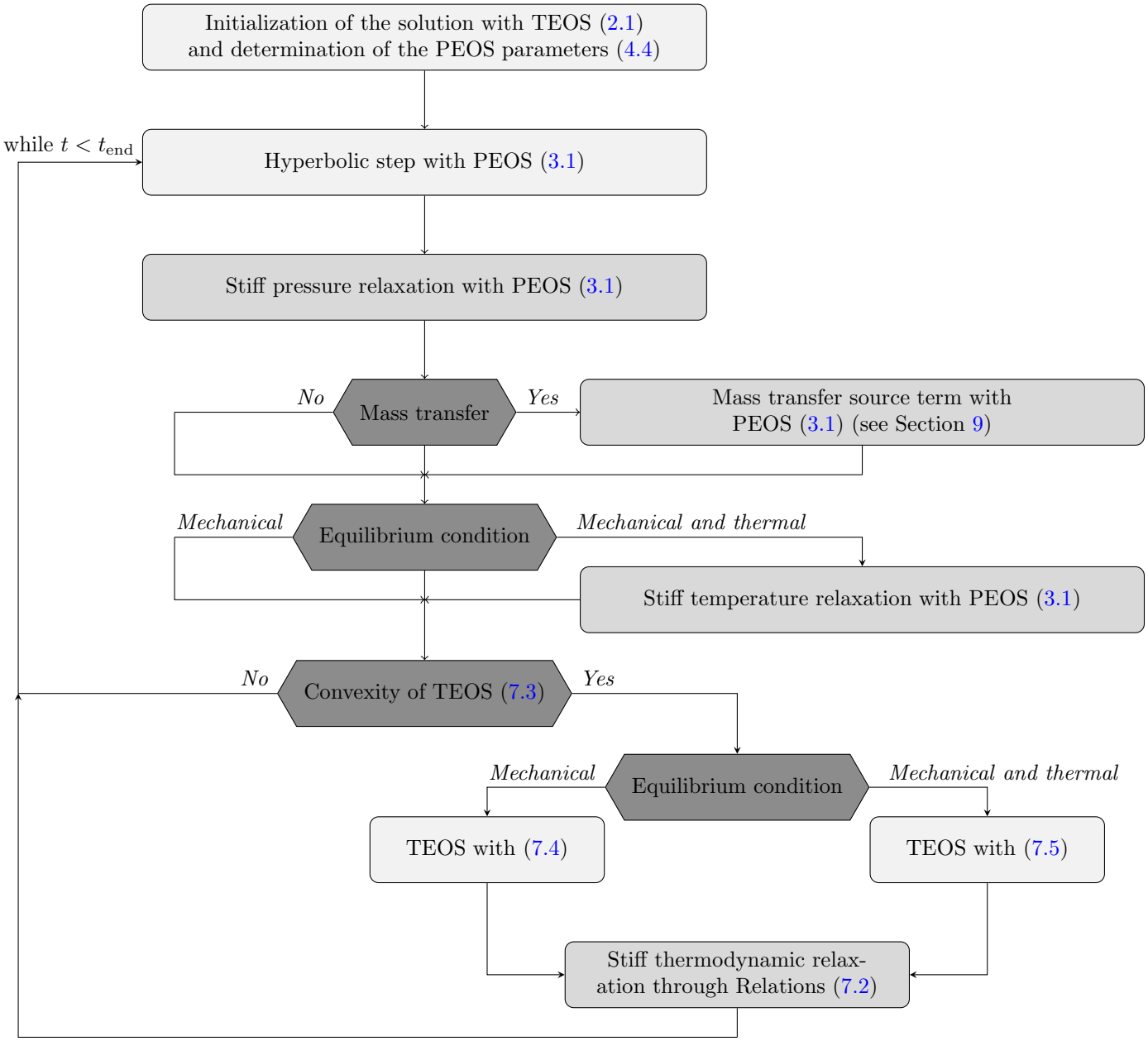

Figure 1: Flowchart of the overall thermodynamic relaxation numerical method with the extended System (4.1)-(4.2). Both versions of the thermodynamic relaxation method are incorporated, *i.e.,* mechanical equilibrium (Section 4) and mechanical-thermal equilibrium (Section 6).

8. Numerical examples

Numerical resolution is addressed using a fractional step method. System (4.1)-(4.2) is solved in the absence of relaxation terms during a time step. It consists of what is referred to as the hyperbolic step, involving the resolution of the Riemann problem and the time evolution stages. In the present contribution, the Riemann problem is solved with the HLLC-type solver provided in Saurel et al. (2009) [28], and the time evolution is computed with a second-order Godunov (1959) [40] type method (see Saurel et al. (2009) [28], Chiapolino et al., 2017 [30]). The various source terms (pressure relaxation, mass transfer, temperature relaxation) are then addressed. Finally, stiff thermodynamic relaxation is achieved to merge TEOS and PEOS.

8.1 Mechanical equilibrium

This section presents an illustration of the present thermodynamic relaxation method for computing a situation involving a material interface. Pressure relaxation is considered but temperature relaxation is omitted. The thermodynamic relaxation method is then used as in its original development (Section 4). The following test is a 1D shock tube initially separating liquid nitromethane (CH_3NO_2) and air. The tube is one meter long, with the initial membrane located at $x = 0.8$ m. The left chamber is initially set at a pressure $p = 2000$ bars, while the right chamber is set at the atmospheric pressure $p = 1$ bar. The initial densities on both sides of the initial interface are $\rho_{CH_3NO_2} = 1134$ kg/m^3 and $\rho_{\text{air}} = 50$ kg/m^3. The initial volume fraction of nitromethane is set to $\alpha_{CH_3NO_2} = 10^{-6}$ in the right chamber and the volume fraction of air is set to $\alpha_{\text{air}} = 10^{-6}$ in the left chamber.

The air is governed by the ideal-gas EOS, which is a reduction of the NASG EOS (3.1) with $b_{\text{air}} = 0$ and $p_{\infty,\text{air}} = 0$. The specific heat coefficient is $C_{v,\text{air}} = 719$ J.kg^{-1}.K^{-1} and the adiabatic coefficient is $\gamma_{\text{air}} = 1.4$, resulting in $R_{\text{air}} = (\gamma_{\text{air}} - 1)\, C_{v,\text{air}} = 287.6$ J.kg^{-1}.K^{-1} . The reference energy is set to $e_{\text{air,ref}} = 0$. The nithomethane is described by the CC EOS (2.1)-(A.1). The corresponding parameters are given in Table A.1 of Appendix A (Saurel et al., 2007 [41]). The computations are performed with a second-order scheme in space and time on a 2000-cell grid, with both the conventional method (TEOS (2.1)) and the thermodynamic relaxation method based on PEOS (3.1). The results are presented in Figure 2.

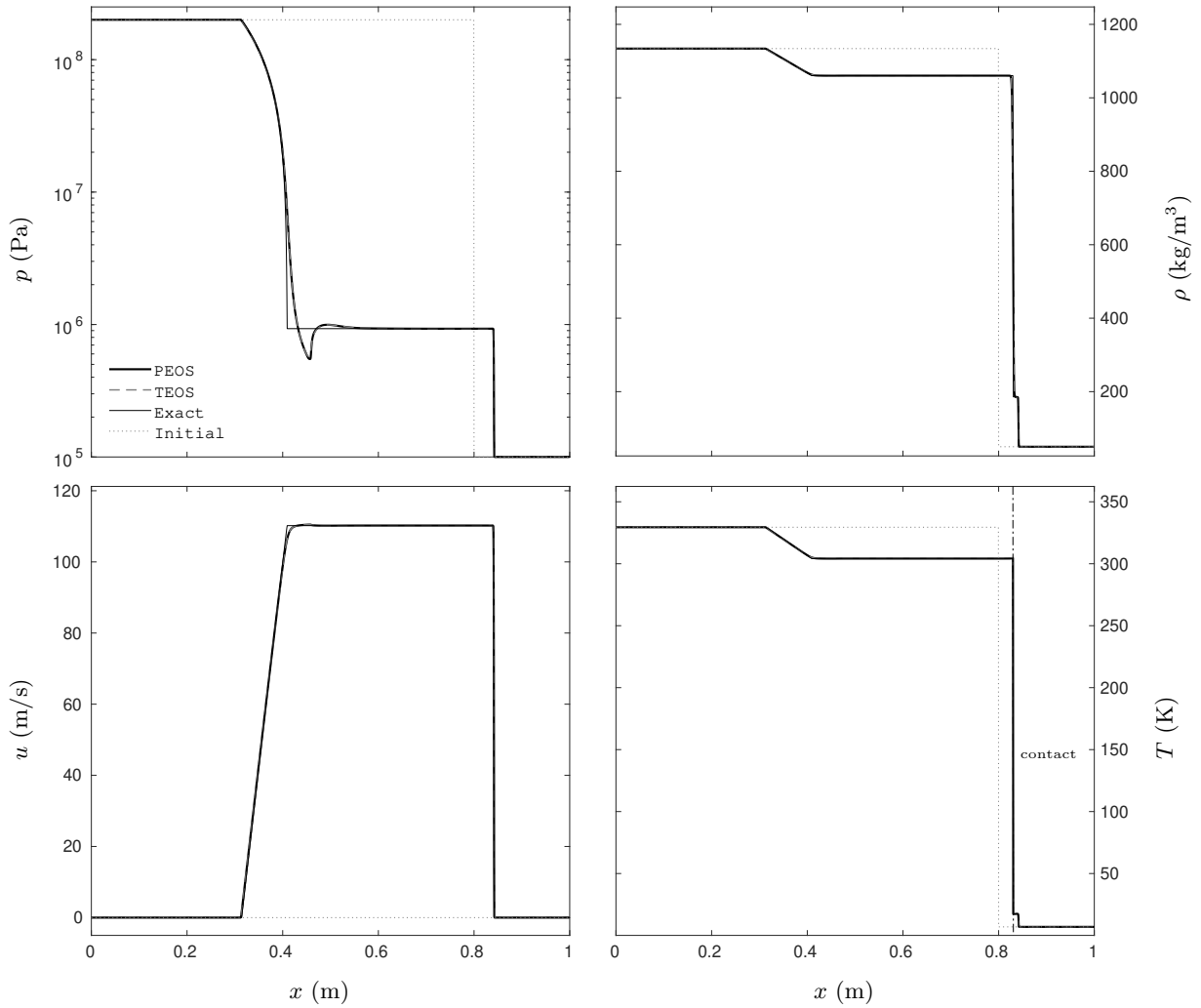

Figure 2: Shock-tube test case with the non-equilibrium model of Saurel et al. (2009) [28]. The thick black lines represent the results computed with the thermodynamic relaxation method (PEOS), and the dashed gray lines correspond to those computed with the conventional method (TEOS). The thin black lines represent the exact solution computed with the Riemann solver of Saurel et al. (1994) [42]. The dotted lines represent the initial conditions. The results are shown at time 276 μs. Since the temperatures are in disequilibrium, the nitromethane temperature is shown on the left of the contact (which is represented by the dash-dotted line), while the air temperature is displayed on the right. The present relaxation method perfectly recovers the target EOS results.

The results computed with the thermodynamic relaxation method using PEOS are merged with those obtained with the conventional method using TEOS. Furthermore, the use of the NASG EOS expressions throughout the numerical code is more computationally efficient than that of CC EOS. The "PEOS" computation is about 2.5 times faster than that with TEOS. The present test case was performed with a sequential implementation. The computation with TEOS required 52 seconds whereas the computation with the thermodynamic relaxation method based on PEOS needed only 21 seconds.

8.2 Mechanical and thermal equilibrium

Temperature relaxation is now considered in addition. The thermodynamic relaxation method is then used in its extended version (Section 6). This section presents an illustration of the present thermodynamic relaxation method for computing a mixture flow. The following test is a 1D shock tube involving liquid nitromethane (CH_3NO_2) and gas TNT products ($C_7H_5N_3O_6$). The tube is one meter long, with the initial membrane located at $x = 0.6$ m. The left chamber is initially set at a pressure $p = 200000$ bars, while the right chamber is set at the atmospheric pressure $p = 1$ bar. The

initial temperatures on both sides of the initial discontinuity are $T = 3000$ K and $T = 300$ K. The initial volume fractions of nitromethane and TNT are set to $\alpha = 0.5$ throughout the whole domain.

The liquid nithomethane is described by the CC EOS (2.1)-(A.1). The corresponding parameters remain the same as before and are given in Table A.1 of Appendix A. The gas TNT products are described by the JWL EOS (2.1)-(B.1), with parameters given in Table B.4 of Appendix B (Massoni et al., 2006 [43]). The non-equilibrium model (4.1) of Saurel et al. (2009) [28] is solved using consecutive pressure and temperature relaxation processes. These cause the solution to converge toward that of the multi-component Euler equations that read:

$$\begin{cases} \dfrac{\partial (\rho Y_k)}{\partial t} + div\left(\rho \mathbf{u} Y_k\right) = 0, \\ \dfrac{\partial \rho}{\partial t} + div\left(\rho \mathbf{u}\right) = 0, \\ \dfrac{\partial (\rho \mathbf{u})}{\partial t} + div\left(\rho \mathbf{u} \otimes \mathbf{u} + p\underline{\underline{\mathbf{I}}}\right) = 0, \\ \dfrac{\partial (\rho E)}{\partial t} + div\left(\rho E + p\right) \mathbf{u} = 0. \end{cases} \tag{8.1}$$

System (8.1) is closed by an appropriate mixture equation of state. This mixture EOS is derived from the equality of pressures p_k between the phases, the equality of temperatures T_k, and the definitions of mixture internal energy e, and mixture specific volume $v = 1/\rho$:

$$\begin{cases} T = T_k, \quad \forall k, \\ p = p_k, \quad \forall k, \\ v = \displaystyle\sum_{k=1}^{N} Y_k v_k\left(p, T\right), \\ e = \displaystyle\sum_{k=1}^{N} Y_k e_k\left(p, T\right). \end{cases} \tag{8.2}$$

The specific volume $v_k = 1/\rho_k$ and internal energy e_k of species k are provided by the EOS of each species. In Relations (8.2), T denotes the mixture temperature. The thermodynamic closure (8.2) assumes that all species evolve in mechanical and thermal equilibrium in their own separate volume. It is interesting to note that Relations (8.2) are equivalent to the mixture law of Dalton when considering a mixture made of ideal gases (Chiapolino et al., 2017 [44]).

The mixture equation of state is derived from System (8.2) and provides the mixture pressure $p\left(v, e, Y_k\right)$ and the mixture temperature $T\left(v, e, Y_k\right)$ as a function of the mixture specific volume v, mixture internal energy e, and mass fractions Y_k. These latter quantities are obtained through the resolution of the multi-component Euler equations (8.1). When dealing with complex MG-type EOSs such as CC (A.1) or JWL (B.1) (Appendix A and Appendix B), it is not possible to express the mixture equation of state in explicit form. This is due to the non-linear dependence of the $p_{k,\text{EOS}}\left(v_k\right)$ and $e_{k,\text{EOS}}\left(v_k\right)$ functions upon the specific volume. Therefore, the mixture pressure p and the mixture temperature T must be computed through the simultaneous resolution of the mixture mass and mixture internal energy relations (8.2) using an iterative method [45], such as Newton-Raphson's. The numerical resolution is performed using a 2×2 matrix.

Figure 3 compares the solution computed by the three models, *i.e.*, the multi-component Euler equations (8.1) where a 2×2 matrix system is solved to compute the mixture pressure and mixture temperature, the non-equilibrium model (4.1) with TEOS where stiff pressure and temperature relaxation solvers are used consecutively, and the augmented

non-equilibrium model (4.1)-(4.2) with PEOS where stiff pressure and temperature relaxation solvers are simplified and accelerated by PEOS. The computations are performed with a second-order scheme in space and time on a 500-cell grid.

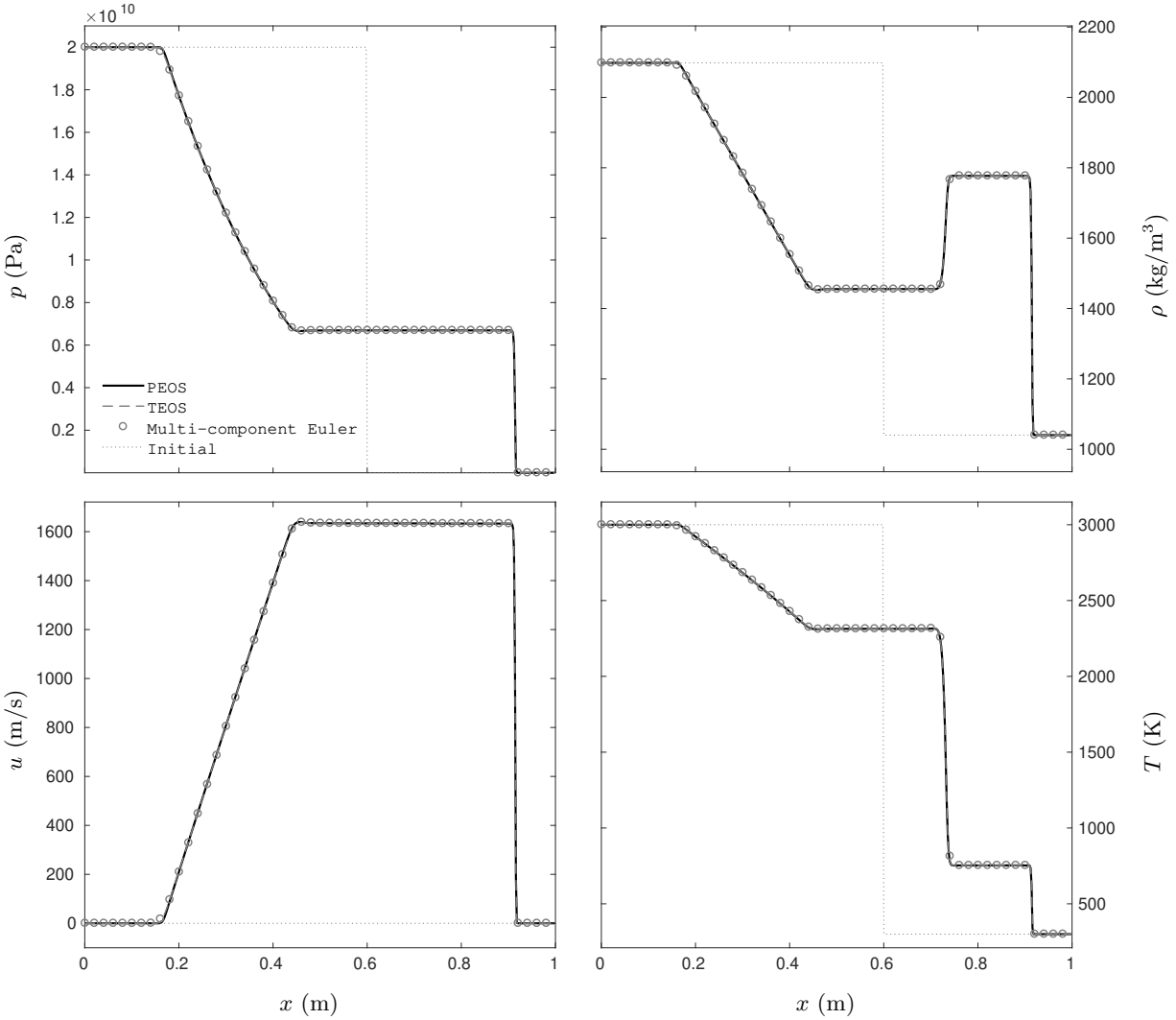

Figure 3: Mixture shock-tube test case. The thick black lines represent the results computed with the thermodynamic relaxation method (PEOS), and the dashed gray lines correspond to those computed with the conventional method (TEOS). The dotted lines represent the initial conditions. The present relaxation method perfectly recovers the target EOS results. In addition, the solution to the multi-component Euler equations is plotted in ∘ symbols. Only 50 symbols out of 500 are plotted for the sake of clarity. The results are shown at time 80 μs.

The results computed with the thermodynamic relaxation method using PEOS are merged with those obtained with the conventional method using TEOS. They are also merged with those computed with the multi-component Euler equations (8.1). The numerical resolution is one more time much more efficient with PEOS. The present test case was performed with a sequential implementation. The conventional computation with TEOS required 10 seconds, whereas the computation with the thermodynamic relaxation method based on PEOS needed only 2 seconds, making the computation 5 times faster.

Both the conventional (TEOS) computation and the computation with the thermodynamic relaxation method based on PEOS are significantly faster than that with the multi-component Euler equations (8.1) that needed 93 seconds. The reason is the complex mixture equation of state that must be extracted from the mixture rules (8.2). When dealing with MG-type EOSs (2.1), such as CC (A.1) or JWL (B.1) (Appendix A and Appendix B), the mixture equation of

state is not expressed explicitly, due to the non-linear dependence of the $p_{k,\mathrm{EOS}}(v_k)$ and $e_{k,\mathrm{EOS}}(v_k)$ functions upon the specific volume. Consequently, the mixture pressure p and the mixture temperature T must be computed through the simultaneous resolution of the mixture mass and mixture internal energy relations (8.2) using an iterative method. This iterative resolution process is a time-consuming computational procedure. However, this difficulty is eliminated with the use of the non-equilibrium model (4.1), which incorporates consecutive pressure and temperature relaxation processes.

9. Mass transfer

In order to address detonations, mass transfer source terms are considered in the flow model. These source terms describe the decomposition of the reactant (R) and the creation of the detonation products (DP). The rate at which these products are created is described by the kinetics of decomposition. For ideal explosives, the detonation zone, *i.e.*, the zone where the mass transfer source terms are activated, is located between the shock corresponding to the von Neumann spike and the Chapman-Jouguet (CJ) point where sonic conditions appear as illustrated in Figure 4.

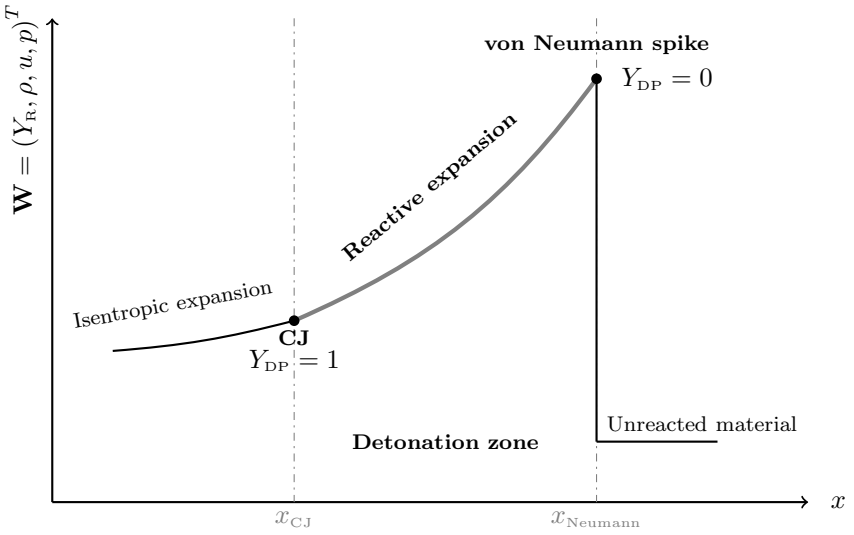

Figure 4: Schematic representation of a 1D detonation of an ideal explosive described by the ZND model. Mass transfer must be present only between the von Neumann spike and the CJ point when dealing with ideal explosives.

9.1 Detonation detection

It is important to highlight that care must be taken to ensure that the mass transfer source term is activated only in the reaction zone. Indeed, in the present context, mixture cells are present due to the numerical dissipation, inherent in all capturing numerical methods. This artificial diffusion tends to spread the shock over several numerical cells and consequently can activate a premature computation of the source term. In this case, the numerical results are considerably corrupted. The von Neumann spike (see Figure 4) must then be correctly detected so that the reaction starts behind the numerical diffusion zone of the shock. A detonation indicator consisting of the following three numerical filters is then

used (Chiapolino et al., 2024 [4]):

$$\begin{cases} \dfrac{p^{n+1}}{p^n} < 1+\epsilon_p, \\ \dfrac{\rho^{n+1}}{\rho^n} < 1+\epsilon_\rho, \\ \left| e^{n+1} - e^n + \dfrac{1}{2}\left(p^{n+1}+p^n\right)\left(v^{n+1}-v^n\right) \right| > \epsilon_{\text{RH}}. \end{cases} \tag{9.1}$$

Computation of the source term is activated for the current numerical cell if these conditions are met. The first condition compares the mixture pressure between two consecutive time steps, denoted by $n+1$ and n. The second condition compares the mixture density. The last condition corresponds to the Hugoniot adiabatic, which is zero only for shocks (Menikoff and Shaw, 2010 [46]). When these conditions are satisfied, the current cell does not carry the (diffused) shock. The parameters $\epsilon_p = \epsilon_\rho = 10^{-2}$ and $\epsilon_{\text{RH}} = 10^{-4}$ J/kg are used. In addition, the computation of the source term is only initiated in the presence of combustible material, through $\alpha_{\text{R}} > \epsilon_\alpha = 10^{-6}$ and $Y_{\text{R}} > \epsilon_Y = 10^{-6}$, and if the mixture pressure in the current numerical cell is high enough: $p > 10^8$ Pa.

9.2 Thermo-chemical solver

Upon completion of the hyperbolic step (resolution of the two-phase flow system (4.1) without source terms), and upon completion of the stiff pressure relaxation process (Section 5), the solution tends to that of the mechanical equilibrium model due to Kapila et al. (2001) [1]. Indeed, the hyperbolic and pressure relaxation steps of System (4.1) provide a numerical method for solving the model proposed by Kapila et al. (2001) [1] in a simple and efficient manner. Let us then analyze the introduction of mass transfer source terms in the mechanical equilibrium model, following Petitpas et al. (2009) [2]. The model of Kapila et al. (2001) [1] with mass transfer terms reads:

$$\begin{cases} \dfrac{\partial \alpha_k}{\partial t} + \mathbf{u}\cdot grad\left(\alpha_k\right) - \left(\dfrac{\rho_l c_l^2 - \rho_k c_k^2}{\rho_k c_k^2/\alpha_k + \rho_l c_l^2/\alpha_l}\right) div(\mathbf{u}) = \dfrac{\rho \dot{Y}_k}{\rho_I} = \dfrac{\dot{m}_k}{\rho_I}, \\ \dfrac{\partial\left(\alpha_k\rho_k\right)}{\partial t} + div\left(\alpha_k\rho_k\mathbf{u}\right) = \rho\dot{Y}_k = \dot{m}_k, \\ \dfrac{\partial\left(\rho\mathbf{u}\right)}{\partial t} + div\left(\left[\rho\mathbf{u}\otimes\mathbf{u} + p\underline{\underline{\mathbf{I}}}\right]\right) = 0, \\ \dfrac{\partial\left(\rho E\right)}{\partial t} + div\left(\left[\rho E + p\right]\mathbf{u}\right) = 0. \end{cases} \tag{9.2}$$

System (9.2) evolves in mechanical equilibrium. However, System (9.2) involves numerical difficulties due to the non-conservative term in the volume-fraction equation. The disequilibrium model (4.1) of Saurel et al. (2009) [28] is consequently used with stiff pressure relaxation to circumvented these numerical difficulties.

In the absence of hydrodynamic terms and in the presence of mass source terms, System (9.2) reads:

$$\begin{cases} \dfrac{\partial \alpha_k}{\partial t} = \dfrac{\rho \dot{Y}_k}{\rho_I} = \dfrac{\dot{m}_k}{\rho_I}, \\ \dfrac{\partial\left(\alpha_k\rho_k\right)}{\partial t} = \rho\dot{Y}_k = \dot{m}_k, \\ \dfrac{\partial\left(\rho\mathbf{u}\right)}{\partial t} = 0, \\ \dfrac{\partial\left(\rho E\right)}{\partial t} = 0. \end{cases} \tag{9.3}$$

The rate at which the detonation products are created is denoted by $\dot{Y}_{\rm DP} = -\dot{Y}_{\rm R}$, which is determined from a given kinetics model. Obviously $\dot{Y}_k = 0$ for inert materials: $k \neq (\mathrm{R}, \mathrm{DP})$. In System (9.3), ρ_I denotes the "interfacial" density. This density is expressed in order to ensure that the flow model satisfies the second law of thermodynamics. Following Saurel et al. (2008) [47], the "interfacial" density ρ_I reads:

$$\rho_I = \frac{\frac{\rho_1 c_1^2}{\alpha_1} + \frac{\rho_2 c_2^2}{\alpha_2}}{\frac{c_1^2}{\alpha_1} + \frac{c_2^2}{\alpha_2}}. \tag{9.4}$$

Knowledge of the kinetics law enables the computation of the mass source term $\dot{m}_k$. The volume fractions α_k and apparent masses $\alpha_k \rho_k$ are updated with a simple first-order integration method.

Nevertheless, the two-phase model used in the numerical method remains the non-equilibrium model (4.1) of Saurel et al. (2009) [28]. Consequently, upon computing the volume fractions α_k and apparent masses $\alpha_k \rho_k$ through the kinetics source terms, the internal energies e_k are updated using the mixture pressure and the associated EOS: $e_k = e_k(p, \rho_k)$, similarly to the energy re-initialization step required during the stiff pressure relaxation process, see Saurel et al. (2009) [28], Chiapolino et al. (2017) [44] for details. This task does not pose any particular difficulty for either TEOS or PEOS. The reader is then referred to the aforementioned references. The solution at this point corresponds to that of the mechanical equilibrium model of Kapila et al. (2001 [1]), with mass transfer, but in the absence of heat transfer between the reactant and the detonation products. Mechanical and thermal equilibrium is computed through an additional relaxation process regarding the temperatures, as seen in Section 6.

10. Numerical examples of detonation with mechanical and thermal equilibrium

The extended thermodynamic relaxation method is now applied to illustrative detonation test cases. As mentioned in the Introduction, the reactive Euler equations with temperature and pressure equilibrium among the phases are commonly used in engineering computations to address detonations in condensed explosives. However, their apparent simplicity has limitations and masks a subtle complexity that can lead to pathological and nonphysical solutions. This issue has been investigated in Chiapolino et al. (2024) [4] and a fundamental existence condition, referred to as Global Exothermic Condition (GEC), of the mechanical-thermal equilibrium model has been provided in order to preserve exothermic detonations in the frame of temperature-pressure equilibrium flow models. Numerical results show that disregarding the GEC (in the reaction zone) leads to pathological solutions. The general expression of the GEC, in the context of mechanical and thermal equilibrium, reads as [4]:

$$\left.\frac{\partial e}{\partial Y_{\rm DP}}\right|_{p,\rho,Y_k'} < \left.\frac{\partial e}{\partial Y_{\rm R}}\right|_{p,\rho,Y_k'}, \tag{10.1}$$

with $Y_k' \neq Y_k$. In order for the mathematical model to provide a non-pathological, and therefore existing detonation, it is necessary that the reaction remains globally exothermic. This condition is expressed through the GEC (10.1), specifically through the careful selection of the parameters of the equations of state [4] that are involved in the formulation of the mixture internal energy e.

In the present contribution the PBXN-109 explosive is used. PBXN-109 is a weakly non-ideal explosive. It is a composite explosive made of 64% hexogen (RDX), 20% of aluminum particles (Al), and 16% of a bounding non-reacting material (PBHT). The solid reactant (R) is described by the CC EOS (2.1)-(A.1) and the associated detonation products

(DP) parameters are described by the JWL EOS (2.1)-(B.1). The corresponding parameters satisfy the GEC (10.1) as shown in Chiapolino et al. (2024) [4]. The CC parameters are given in Table A.2 of Appendix A. These parameters lead to an excellent agreement with the experimental Hugoniot data, as will be seen a bit further (Figure 7). Among the CC parameters, the constant $E_{k,2}$ is of particular interest. The fact that $E_{k,2} = 0$ guarantees convexity of the CC formulation, under conditions that $T_k > 0$ and $v_k > 0$, as shown in Chiapolino et al. (2024) [4]. However, the combination of an accurate Hugoniot adiabat and convexity may not be found for every material. For example, copper will be used in the forthcoming section and requires $E_{k,2} > 0$ to match the associated experimental Hugoniot data (Figure 7). It should also be noted that the reference energy $e_{\mathrm{R,ref}}$ is computed so the initial (0) internal energy of the solid reactant is zero: $e_{\mathrm{R},0}\left(p_0, T_0\right) = 0$. The combination of Relations (2.1) and (A.1) leads to $e_{\mathrm{R,ref}} = 0$. The energy released by the combustion is then transferred to the reference energy of the detonation products $e_{\mathrm{DP,ref}}$ (third relation of (B.2), see Appendix B).

The JWL parameters used to describe the detonation products are also provided in Chiapolino et al. (2024) [4]. They are determined using the thermochemical code Cheetah (Fried, 1998 [48], Lu, 2001 [49]), which provides the CJ state for a given material density. Yet, the heat capacity is modified in order to maintain a convex formulation, also under condition that $T_k > 0$ and $v_k > 0$. The demonstration is provided in Chiapolino et al. (2024) [4] as well. The JWL parameters are given in Table B.5 of Appendix B. The present JWL description of the detonation products of the PBXN-109 involves a reasonable inaccuracy on the pressure at the CJ point: 2%, but a larger error on the temperature at the CJ point: 17%. This is due to the heat capacity of the detonation products that was deliberately lowered at $C_{v,\mathrm{DP}} = 1000$ J/kg/K to ensure convexity of the JWL EOS [4]. This inaccuracy is reduced to 8.6% when $C_{v,\mathrm{DP}} = 1960$ J/kg/K, provided by Cheetah, is used. As the present contribution is solely intended to extend the thermodynamic relaxation method, this temperature error is not a significant issue.

In Neron et al. (2023) [27], the same detonation products of PBXN-109 are used in an underwater explosion test, wherein the materials are in thermal disequilibrium. It is shown that the conventional computation (TEOS) and the computation with the thermodynamic relaxation method based on PEOS provide the same results up to a specific point where TEOS becomes non-convex due to its $C_{v,\mathrm{DP}}$ value of 1960 J/kg/K, which ultimately leads to computational failure. Nevertheless, the computation with the thermodynamic relaxation method based on PEOS is able to proceed and yields consistent results. When the $C_{v,\mathrm{DP}}$ value is modified to 1000 J/kg/K to ensure convexity of the JWL EOS, the conventional computation with TEOS and the computation with the thermodynamic relaxation method based on PEOS yield identical results throughout the entire simulation [27].

10.1 One-dimensional illustration

First, a 1D detonation test is performed. The 1D numerical test consists of a 30-cm long tube with a fine mesh of 3000 cells. It is initially filled with PBXN-109, which serves as the solid reactant. The initial (0) conditions are as follows: $p_0 = 10^5$ Pa, $T_0 = 298$ K, and $Y_{\mathrm{R},0} = 1 - 10^{-6}$. These conditions, as prescribed by the associated EOS, result in an initial solid density of $\rho_{\mathrm{R},0} = 1/v_{\mathrm{R},0} = 1666$ kg/m^3, in agreement with experimental data. The detonation is initiated with the help of a piston impacting the left side of the tube at 200 m/s. For the sake of simplicity, the kinetics of decomposition given in Fickett and Davis (1979) [50] is used: $\dot{Y}_{\mathrm{DP}} = \xi\sqrt{\left(1 - Y_{\mathrm{DP}}\right)}$ with $\xi = 2 \times 10^6$ s^{-1}. The results computed with both the conventional computation (TEOS) and the computation with the thermodynamic relaxation method based on PEOS are compared in Figure 5.

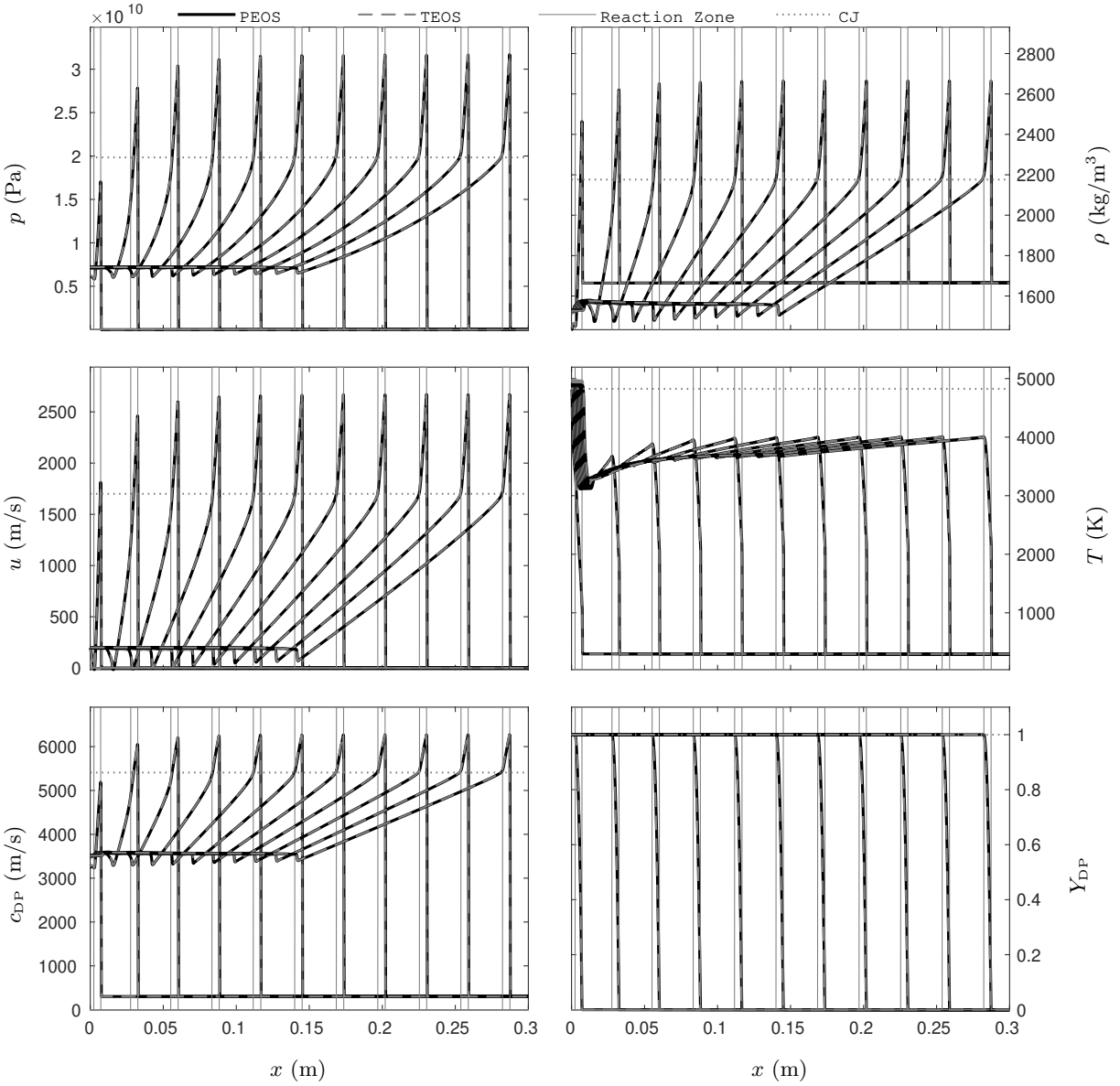

Figure 5: One-dimensional detonation of PBXN-109. The thick black lines represent the results computed with the thermodynamic relaxation method (PEOS), and the dashed gray lines correspond to those computed with the conventional method (TEOS). The thin gray lines represent the detonation zone (plotted only for the "PEOS" computation for the sake of clarity) where the mass-transfer source terms are activated. The prescribed CJ state (Table B.5) is represented by the horizontal dotted lines. The solution is shown at time intervals of 4 μs, with the first and final time being 2 μs and 42 μs. The present relaxation method perfectly recovers the target EOS results.

The results computed with the thermodynamic relaxation method using PEOS are merged with those obtained with the conventional method using TEOS. Moreover, the "PEOS" computation is about 4.3 times faster than that with TEOS. The present test case was performed with a sequential implementation. The conventional computation with TEOS required 15 minutes and 18 seconds whereas the computation with the thermodynamic relaxation method based on PEOS needed only 3 minutes and 32 seconds.

The CJ state is correctly computed, except for the temperature as mentioned previously, and a stationary detonation appears. The reactive expansion occurs from the von Neumann spike to the CJ point, where the combustion is complete, and a conventional isentropic expansion takes place. The computed detonation speed is 7109 m/s, which is close to the

prescribed one (7108.23 m/s, Table B.5). A close-up view of the solution in the reaction zone is shown in Figure 6. The results are compared with the ZND solution as well, which is computed from the stationary reactive Euler equations (8.1) (with $\rho\dot{Y}_{\mathrm{DP}}$ as a source term on the right-hand side of the first equation), providing the stationary solution within the reaction zone. The ZND system reads (Chiapolino et al., 2024 [4]):

$$\begin{cases} \dfrac{\partial \overline{u}}{\partial x} = \dfrac{-\left(\left.\frac{\partial e}{\partial Y_{\mathrm{DP}}}\right|_{p,\rho,Y_k'} - \left.\frac{\partial e}{\partial Y_{\mathrm{R}}}\right|_{p,\rho,Y_k'}\right)\dot{Y}_{\mathrm{DP}}\left.\frac{\partial p}{\partial e}\right|_{\rho,Y_k}}{\rho\left(c^2-\overline{u}^2\right)}, \\ \dfrac{\partial \rho}{\partial x} = -\dfrac{\rho}{\overline{u}}\dfrac{\partial \overline{u}}{\partial x}, \\ \dfrac{\partial p}{\partial x} = -\rho\overline{u}\dfrac{\partial \overline{u}}{\partial x}, \\ \dfrac{\partial Y_{\mathrm{DP}}}{\partial x} = \dfrac{\dot{Y}_{\mathrm{DP}}}{\overline{u}}, \end{cases} \tag{10.2}$$

where $\overline{u} = D - u$ is the relative speed, which is the difference between the speed of the detonation D and the mixture velocity u. The mixture sound speed is denoted by c. Excellent agreement with the ZND solution in the reaction zone is obtained.

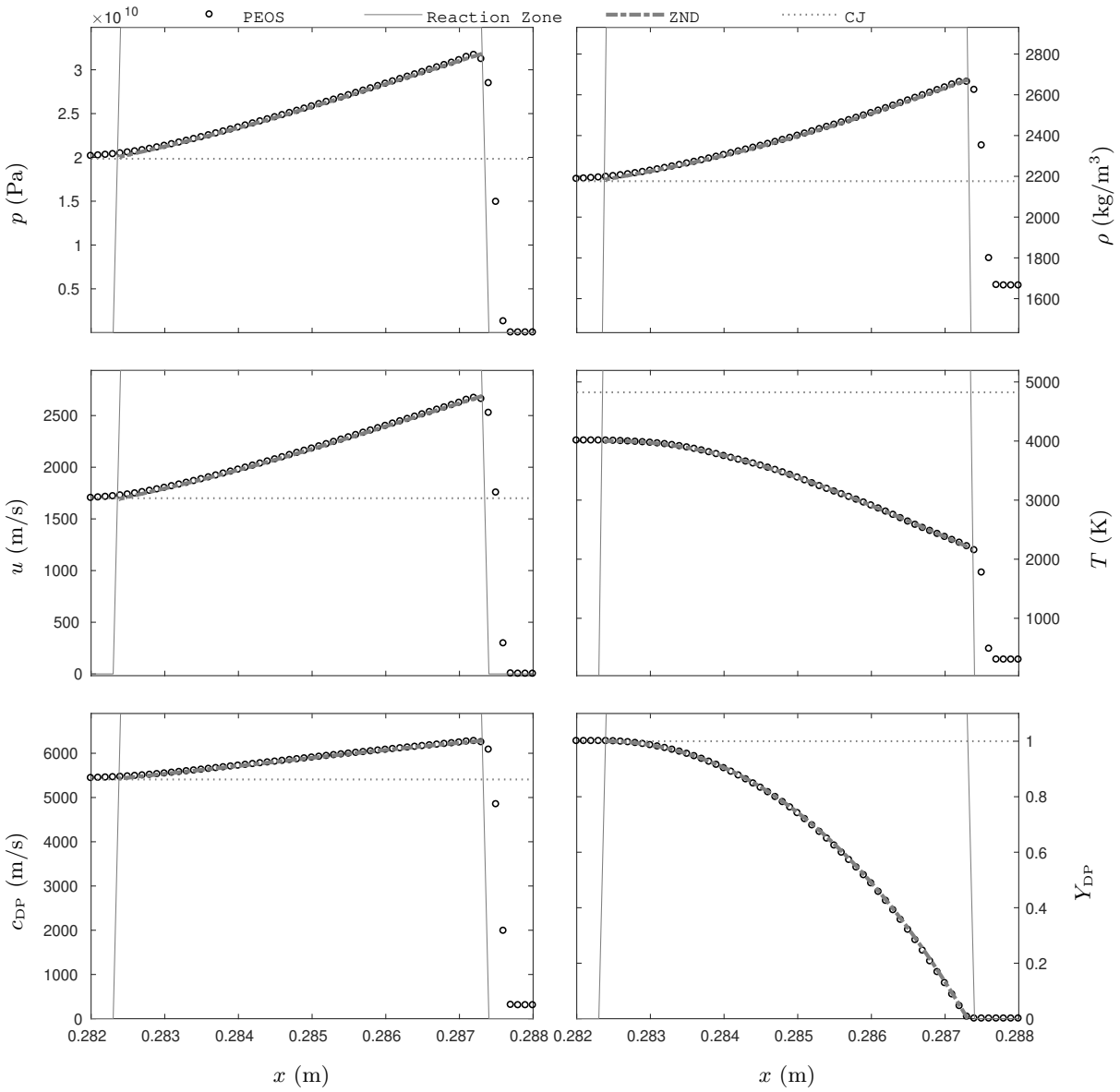

Figure 6: Close-up view of the "PEOS-with-thermodynamic-relaxation" solution of Figure 5 in the reaction zone. The results are compared with the ZND solution at the final time 42 μs.

10.2 Two-dimensional illustration

A 2D illustrative test case is now performed. Mechanical and thermal equilibrium is considered between the PBXN-109 reactant and its associated products. Furthermore, the present test case involves inert materials and consequently material interfaces. Both versions of the thermodynamic relaxation method are then used, *i.e.,* mechanical equilibrium (Section 4) and mechanical-thermal equilibrium (Section 6). The test consists of a copper (Cu) projectile impacting at 1000 m/s an envelope made of copper as well, and containing the solid PBXN-109 explosive. Air is present in the surroundings, and is described by the ideal-gas equation of state (Section 8.1).

The PBXN-109 remains described by the CC EOS (2.1)-(A.1) with parameters given in Table A.2. These parameters have been determined in Chiapolino et al. (2024) [4] to match the experimental dynamic adiabatic. The behavior of a

solid material under shock loading is indeed described by the Hugoniot adiabatic related to:

$$D = c_{k,0} + a_k u, \tag{10.3}$$

where $c_{k,0}$ is the speed of sound of the unshocked (0) solid and a_k is a dimensionless constant specific to the solid under consideration. Relation (10.3) is supported by experimental data providing the $c_{k,0}$ and a_k parameters. For the solid PBXN-109, these parameters were determined experimentally in [4] and are $c_{\mathrm{R},0} = 2231$ m/s and $a_{\mathrm{R}} = 1.845$. For copper, they have been determined using the experimental data provided by the "Shock Wave DataBase" [51] and the least squares method, resulting in $c_{\mathrm{copper},0} = 3350$ m/s and $a_{\mathrm{copper}} = 1.2536$. The copper is described by the CC EOS as well. The corresponding parameters have been determined using the $c_{\mathrm{copper},0}$ and a_{copper} coefficients to math the experimental dynamic adiabatic, and are given in Table A.3 of Appendix A. Figure 7 presents a comparison between the CC EOS with associated parameters for the solid PBXN-109 and copper, with the corresponding Hugoniot data. Excellent agreement is found for both solids.

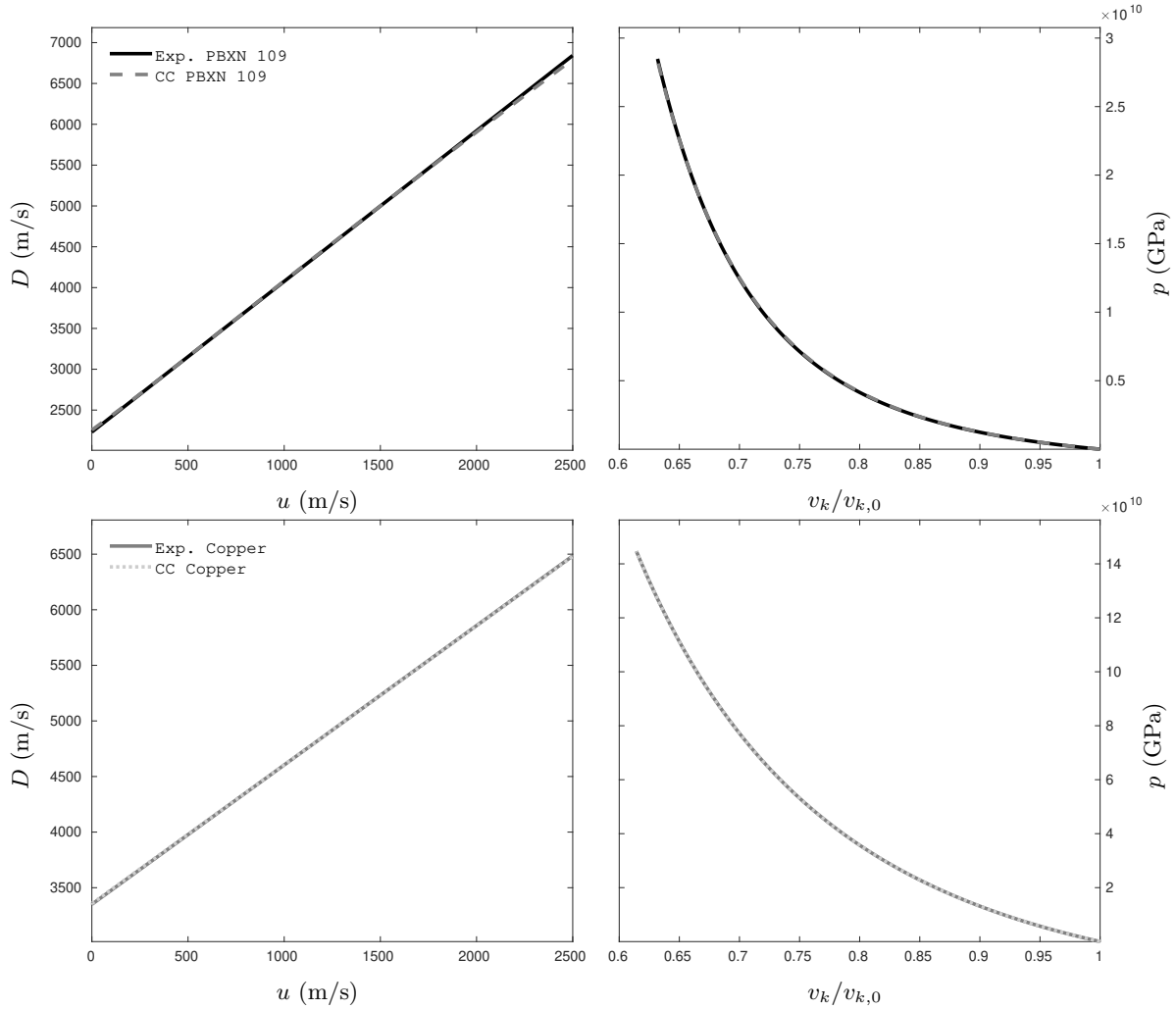

Figure 7: Comparison of the CC EOS for the solid PBXN 109 (top plots) and copper (bottom plots) with the Hugoniot data. For the solid PBXN-109, the CC EOS is fitted with $c_{\mathrm{R},0} = 2231$ m/s and $a_{\mathrm{R}} = 1.845$ from experiment [4]. For copper, the CC EOS is fitted with $c_{\mathrm{copper},0} = 3350$ m/s and $a_{\mathrm{copper}} = 1.2536$ from the "Shock Wave DataBase" [51].

As the numerical test is only intended to be illustrative, the numerical domain is a square with a surface area of 1×1

m^2. The solid PBXN-109 is a square with dimensions 0.6×0.6 m^2. The copper envelop is also a square with dimensions 0.7×0.7 m^2. Its thickness is 0.05 m. The copper projectile is a rectangle with dimensions of 0.3×0.1 m^2. It is initially separated from the copper envelope. The initial velocity in the longitudinal direction is 1000 m/s. The mesh is composed of 421950 unstructured triangles. Non-reflective boundary conditions are considered.

For the sake of simplicity, the kinetics of decomposition given in Fickett and Davis (1979) [50]: $\dot{Y}_{\text{DP}} = \xi\sqrt{(1 - Y_{\text{DP}})}$ is used one more time with $\xi = 0.8 \times 10^6$ s^{-1}. The solution is computed with a second-order Godunov (1959) [40] type method [28, 30, 52]. Moreover, the numerical capture of the material interfaces is improved using the sharpening method developed by Chiapolino et al. (2017) [30]. Figure 8 displays the 2D results computed with the thermodynamic relaxation method based on PEOS.

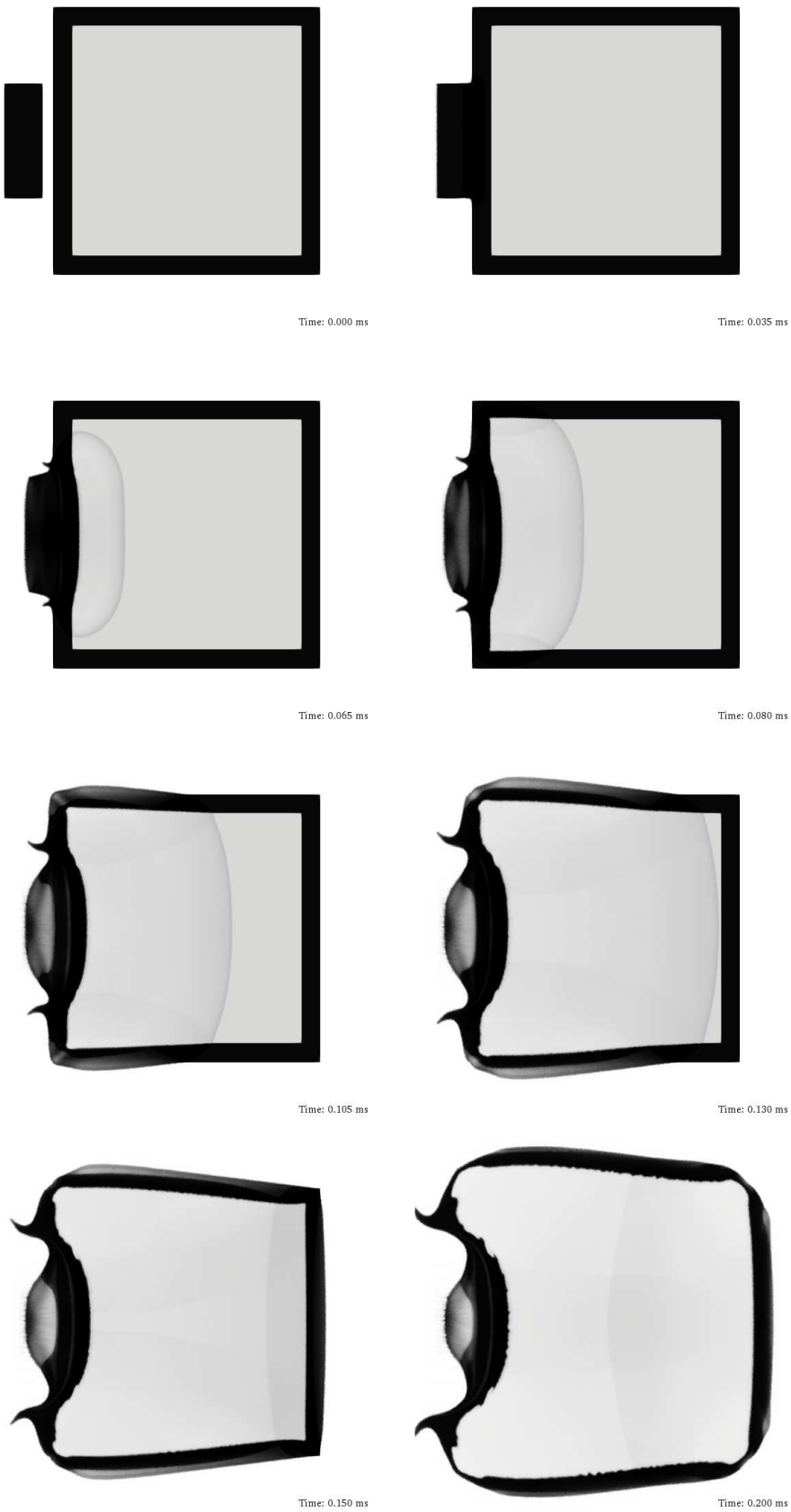

Figure 8: Two-dimensional detonation of PBXN-109 computed with the thermodynamic relaxation method based on PEOS. The figure depicts the temporal evolution of the mixture density ρ, showing the propagation of a detonation wave.

Figure 8 depicts the evolution of the detonation front, which propagates in the explosive in a direction toward the right. The final two images show the propagation of the shock wave following its reflection on the right side of the envelope. The solid PBXN-109 is fully burnt. A comparison between the conventional computation (TEOS) and the computation with the thermodynamic relaxation method based on PEOS is presented in Figure 9, which plots the 2D results on the x-axis along the centerline.

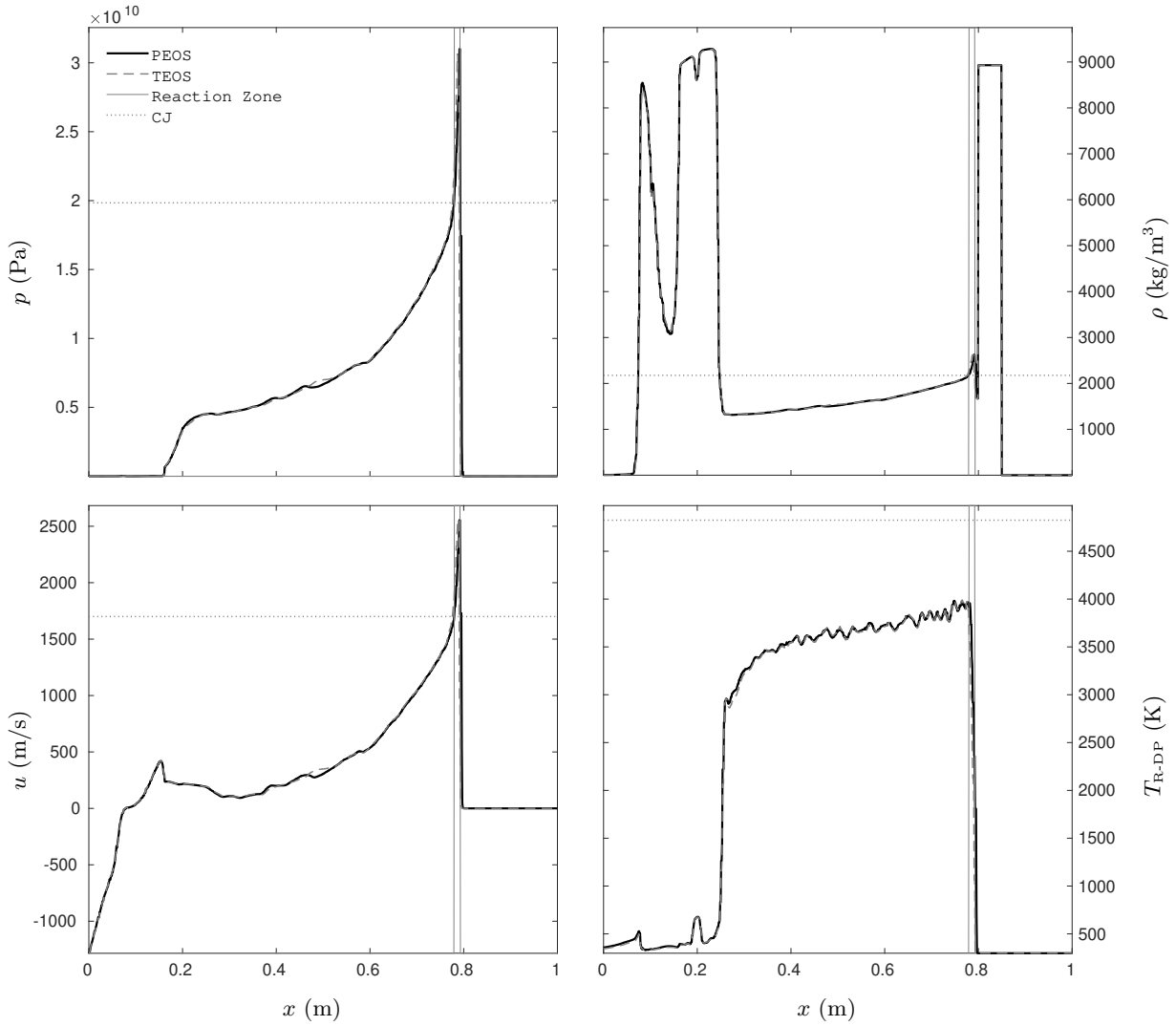

Figure 9: 2D results of Figure 8 plotted on the x-axis along the centerline. Comparison between the conventional computation (TEOS) and the computation with the thermodynamic relaxation method based on PEOS. The results are presented at time 0.130 ms. The thick black lines represent the results computed with the thermodynamic relaxation method (PEOS), and the dashed gray lines correspond to those computed with the conventional method (TEOS). The thin gray lines represent the detonation zone (plotted only for the "PEOS" computation for the sake of clarity) where the mass-transfer source terms are activated. The prescribed CJ state (Table B.5) is represented by the horizontal dotted lines.

The results computed with the thermodynamic relaxation method using PEOS are in excellent agreement with those obtained with the conventional method using TEOS. Moreover, the "PEOS" computation is more than 5 times faster than the "TEOS" computation. The present test case was performed with a parallel implementation using MPI architecture and 60 CPU cores. The conventional computation with TEOS required 5 hours and 18 minutes whereas the computation with the thermodynamic relaxation method based on PEOS needed only 1 hour.

11. Conclusion

The present paper has built upon the thermodynamic relaxation method recently developed in Neron et al. (2023) [27] to encompass both mechanical and thermal equilibrium, thus enabling the treatment of detonation waves in condensed explosives in the frame of pressure and temperature equilibrium models. Most engineering tools dealing with detonation waves in condensed explosives are indeed based on the reactive Euler equations, which involve a thermodynamic closure based on temperature and pressure equilibrium conditions. An extension of the thermodynamic relaxation is then necessary and has been developed in the present contribution.

A condensed explosive is always confined by an external material. The treatment of material interfaces is then essential. Detonation computations have then been addressed with the non-equilibrium model of Saurel et al. (2009) [28]. This model is able to address material interfaces as its solution tends, through stiff pressure relaxation processes, to that of the mechanical equilibrium model of Kapila et al. (2001) [1]. Mass transfer and temperature relaxation terms are added to the multiphase model to recover the solution to the reactive Euler equations in the detonation zone.

The thermodynamic relaxation method is then used in both its original version to address material interfaces, and its extended version to cope with mechanical and thermal equilibrium. This thermodynamic relaxation method allows to compute interfacial flows and mixture flows with sophisticated equations of state such as MG formulations, which include the CC and JWL EOSs. The present method has several key features:

- It automatically achieves the prolongation of the EOS, which significantly improves the robustness of the computations, as most considered EOSs have a limited range of validity.
- It is about 5 times faster than the computations achieved with the original EOS, in the mechanical-thermal equilibrium multiphase flow examples considered herein.
- It is versatile, in the sense that various flow models can be considered with this method.

In the present contribution, JWL and CC EOSs have been considered in the context of detonation computations of ideal explosives. However, the method may be adapted to other complex equations of state such as the Becker-Kistiakowsky-Wilson (BKW) EOS [53–55] following Neron and Saurel (2024) [56]. Other future work includes extensions to extra physics, such as cubic EOSs, as well as virial ones, each one having important interest and difficulties in different technical areas.

Declaration of Interests

The authors report no conflict of interest.

Availability of data

The data that support the findings of this study are available within the article.

Appendix A. CC functions

The Cochran-Chan (CC) EOS is widely used to model the thermodynamics of the condensed phase. The various functions used in (2.1) are denoted by the subscript "CC" and read as [4],

$$\begin{cases} p_{k,\mathrm{EOS}}\left(v_k\right) = p_{k,\mathrm{CC}}\left(v_k\right) = A_{k,1}\left(\dfrac{v_k}{v_{k,0}}\right)^{-E_{k,1}} - A_{k,2}\left(\dfrac{v_k}{v_{k,0}}\right)^{-E_{k,2}}, \\ e_{k,\mathrm{EOS}}\left(v_k\right) = e_{k,\mathrm{CC}}\left(v_k\right) = -\dfrac{A_{k,1}v_{k,0}}{1-E_{k,1}}\left(\left(\dfrac{v_k}{v_{k,0}}\right)^{1-E_{k,1}} - 1\right) + \dfrac{A_{k,2}v_{k,0}}{1-E_{k,2}}\left(\left(\dfrac{v_k}{v_{k,0}}\right)^{1-E_{k,2}} - 1\right) - C_{v,k}T_0 + e_{k,\mathrm{ref}}, \\ \dfrac{\mathrm{d}p_{k,\mathrm{EOS}}\left(v_k\right)}{\mathrm{d}v_k} = \dfrac{\mathrm{d}p_{k,\mathrm{CC}}\left(v_k\right)}{\mathrm{d}v_k} = -\dfrac{A_{k,1}E_{k,1}}{v_{k,0}}\left(\dfrac{v_k}{v_{k,0}}\right)^{-1-E_{k,1}} + \dfrac{A_{k,2}E_{k,2}}{v_{k,0}}\left(\dfrac{v_k}{v_{k,0}}\right)^{-1-E_{k,2}}, \end{cases} \tag{A.1}$$

where $A_{k,1}$, $A_{k,2}$, $E_{k,1}$, and $E_{k,2}$ are parameters determined from the reference Hugoniot curve of the tested material k. Subscript "0" indicates the reference state data used to calibrate these parameters, *i.e.*, the standard unreacted state. The term $e_{k,\mathrm{ref}}$ represents the reference energy. The CC EOS is commonly used to describe the solid reactant. The various CC thermodynamic parameters used in this paper are listed in the following tables.

T_0 (K)	$v_{k,0}$ (m^3/kg)	$e_{k,\mathrm{ref}}$ (J/kg)	Γ_k	$A_{k,1}$ (GPa)	$A_{k,2}$ (GPa)	$E_{k,1}$	$E_{k,2}$	$C_{v,k}$ (J/kg/K)
300	1/1134	0	1.19	0.819181	1.50835	4.52969	1.42144	2000

Table A.1: Parameters of the CC EOS for liquid nitromethane ($k = \mathrm{CH_3NO_2}$) [41].

T_0 (K)	$v_{k,0}$ (m^3/kg)	$e_{k,\mathrm{ref}}$ (J/kg)	Γ_k	$A_{k,1}$ (GPa)	$A_{k,2}$ (GPa)	$E_{k,1}$	$E_{k,2}$	$C_{v,k}$ (J/kg/K)
298	1/1666	0	1.2	1.0	1.7922629	6.7333333	0	1330

Table A.2: Parameters of the CC EOS for the solid unreacted PBXN-109 ($k = \mathrm{R}$) [4].

T_0 (K)	$v_{k,0}$ (m^3/kg)	$e_{k,\mathrm{ref}}$ (J/kg)	Γ_k	$A_{k,1}$ (GPa)	$A_{k,2}$ (GPa)	$E_{k,1}$	$E_{k,2}$	$C_{v,k}$ (J/kg/K)
298	1/8930	0	0.7965	503.5075	504.3235	2.1	1.9	385

Table A.3: Parameters of the CC EOS for copper ($k = \mathrm{Cu}$).

Appendix B. JWL functions

The JWL EOS is widely used to model the thermodynamics of the detonation products. The various functions denoted by the subscript "JWL" read as [4],

$$\begin{cases} p_{k,\mathrm{EOS}}\left(v_k\right) = p_{k,\mathrm{JWL}}\left(v_k\right) = A_k e^{-R_{k,1}\frac{v_k}{v_{\mathrm{R},0}}} + B_k e^{-R_{k,2}\frac{v_k}{v_{\mathrm{R},0}}} + k_k\left(\dfrac{v_{\mathrm{R},0}}{v_k}\right)^{\Gamma_k+1}, \\ e_{k,\mathrm{EOS}}\left(v_k\right) = e_{k,\mathrm{JWL}}\left(v_k\right) = \dfrac{A_k v_{\mathrm{R},0}}{R_{k,1}} e^{-R_{k,1}\frac{v_k}{v_{\mathrm{R},0}}} + \dfrac{B_k v_{\mathrm{R},0}}{R_{k,2}} e^{-R_{k,2}\frac{v_k}{v_{\mathrm{R},0}}} + \dfrac{k_k v_{\mathrm{R},0}}{\Gamma_k}\left(\dfrac{v_{\mathrm{R},0}}{v_k}\right)^{\Gamma_k} + e_{k,\mathrm{ref}}, \\ \dfrac{\mathrm{d}p_{k,\mathrm{EOS}}\left(v_k\right)}{\mathrm{d}v_k} = \dfrac{\mathrm{d}p_{k,\mathrm{JWL}}\left(v_k\right)}{\mathrm{d}v_k} = -\dfrac{A_k R_{k,1}}{v_{\mathrm{R},0}} e^{-R_{k,1}\frac{v_k}{v_{\mathrm{R},0}}} - \dfrac{B_k R_{k,2}}{v_{\mathrm{R},0}} e^{-R_{k,2}\frac{v_k}{v_{\mathrm{R},0}}} - \left(1+\Gamma_k\right)\dfrac{k_k v_{\mathrm{R},0}}{v_k^2}\left(\dfrac{v_{\mathrm{R},0}}{v_k}\right)^{\Gamma_k}, \end{cases} \tag{B.1}$$

where A_k, B_k, $R_{k,1}$, $R_{k,2}$, and k_k are fitted parameters depending on the considered material k. In these relations, $v_{\mathrm{R},0}$ is the specific volume of the solid reactant (R) in the reference state (0). The term $e_{k,\mathrm{ref}}$ denotes the reference energy. For the detonation products ($k = \mathrm{DP}$), the k_{DP} and $e_{\mathrm{DP,ref}}$ parameters are determined using the CJ state,

$$\begin{cases} k_{\mathrm{DP}} = \left(p_{\mathrm{CJ}} - p_{\mathrm{DP},1}\left(v_{\mathrm{CJ}}\right) - \dfrac{\Gamma_{\mathrm{DP}} C_{v,\mathrm{DP}} T_{\mathrm{CJ}}}{v_{\mathrm{CJ}}}\right)\left(\dfrac{v_{\mathrm{CJ}}}{v_{\mathrm{R},0}}\right)^{\Gamma_{\mathrm{DP}}+1} = C_{\mathrm{DP}} - \dfrac{\Gamma_{\mathrm{DP}} C_{v,\mathrm{DP}} T_{\mathrm{CJ}}}{v_{\mathrm{CJ}}}\left(\dfrac{v_{\mathrm{CJ}}}{v_{\mathrm{R},0}}\right)^{\Gamma_{\mathrm{DP}}+1}, \\ p_{\mathrm{DP},1}\left(v_{\mathrm{DP}}\right) = A_{\mathrm{DP}} e^{-R_{\mathrm{DP},1}\frac{v_{\mathrm{DP}}}{v_{\mathrm{R},0}}} + B_{\mathrm{DP}} e^{-R_{\mathrm{DP},2}\frac{v_{\mathrm{DP}}}{v_{\mathrm{R},0}}}, \\ e_{\mathrm{DP,ref}} = e_{\mathrm{CJ}} - \dfrac{A_{\mathrm{DP}} v_{\mathrm{R},0}}{R_{\mathrm{DP},1}} e^{-R_{\mathrm{DP},1}\frac{v_{\mathrm{CJ}}}{v_{\mathrm{R},0}}} - \dfrac{B_{\mathrm{DP}} v_{\mathrm{R},0}}{R_{\mathrm{DP},2}} e^{-R_{\mathrm{DP},2}\frac{v_{\mathrm{CJ}}}{v_{\mathrm{R},0}}} - v_{\mathrm{CJ}} \dfrac{p_{\mathrm{CJ}} - p_{\mathrm{DP},1}\left(v_{\mathrm{CJ}}\right)}{\Gamma_{\mathrm{DP}}}, \\ v_{\mathrm{CJ}} = v_{\mathrm{R},0} - p_{\mathrm{CJ}}\left(\dfrac{v_{\mathrm{R},0}}{D}\right)^2, \\ e_{\mathrm{CJ}} = \dfrac{p_{\mathrm{CJ}}}{2}\left(v_{\mathrm{R},0} - v_{\mathrm{CJ}}\right) + e_{\mathrm{R},0}. \end{cases} \tag{B.2}$$

The last two relations of (B.2) result from the CJ theory, which was developed for an infinitesimally thin detonation (see for instance Fickett and Davis, 1979 [50]). They correspond to the shock relations between the initial state (0), which is the unreacted solid (R), and the CJ state, wherein the gases reach sonic velocity (in the frame of the leading shock wave) as the reaction ceases. The detonation speed is denoted by D. The term $e_{\mathrm{R},0}$ denotes the internal energy of the solid reactant in the standard unreacted state. It should be noted that the last relation supposes that the pressure in the CJ state is significantly greater than that in the initial state: $p_{\mathrm{CJ}} \gg p_0$. The term C_{DP}, present in the first relation of (B.2), is an additional parameter depending on the considered detonation products. The JWL EOS is indeed commonly used to describe detonation products (DP). The various JWL thermodynamic parameters used in this paper are listed in the following tables.

$v_{\mathrm{R},0}$ (m^3/kg)	Γ_k	$C_{v,k}$ (J/kg/K)	A_k (GPa)	B_k (GPa)	C_k (GPa)	$R_{k,1}$	$R_{k,2}$
1/1605	0.290	2399	492.6	5.950	0.924	4.730	1.060

D (m/s)	p_{CJ} (GPa)	T_{CJ} (K)
6737	18.18	3712

Table B.4: Parameters of the JWL EOS for the detonation products of TNT ($k = \mathrm{C_7H_5N_3O_6}$) [43].

A_k (GPa)	B_k (GPa)	C_k (GPa)	$R_{k,1}$	$R_{k,2}$	Γ_k	$C_{v,k}$ (J/kg/K)	p_{CJ} (GPa)	T_{CJ} (K)	D ($\mathrm{m.s^{-1}}$)
1235.851	18.289	1.76	6.104	1.434	0.226	1000	19.842	4824.79	7108.23

Table B.5: Parameters of the JWL EOS for the detonation products of PBXN-109 ($k = \mathrm{DP}$) [4].

References

[1] A. Kapila, R. Menikoff, J. Bdzil, S. Son, D. Stewart, Two-phase modeling of deflagration-to-detonation transition in granular materials: Reduced equations, Physics of Fluids 13 (10) (2001) 3002–3024. doi:doi:10.1063/1.1398042.

[2] F. Petitpas, R. Saurel, E. Franquet, A. Chinnayya, Modelling detonation waves in condensed energetic materials: Multiphase CJ conditions and multidimensional computations, Shock Waves 19 (5) (2009) 377–401. doi:https://doi.org/10.1007/s00193-009-0217-7.

[3] R. Saurel, F. Fraysse, D. Furfaro, E. Lapébie, Multiscale multiphase modeling of detonations in condensed energetic materials, Computers & Fluids 159 (2017) 95–111. doi:https://doi.org/10.1016/j.compfluid.2018.03.054.

[4] A. Chiapolino, R. Saurel, S. Bodard, Existence condition for detonations in condensed explosives with pressure–temperature equilibrium models, Physics of Fluids 36 (11) (2024) 116124. doi:https://doi.org/10.1063/5.0238486.

[5] S. Cochran, J. Chan, Shock initiation and detonation models in one and two dimensions, Tech. rep., California Univ., Livermore (USA). Lawrence Livermore Lab. (1979).

[6] E. Lee, C. Tarver, Phenomenological model of shock initiation in heterogeneous explosives, The Physics of Fluids 23 (12) (1980) 2362–2372. doi:https://doi.org/10.1063/1.862940.

[7] A. Sileem, D. Kassoy, A. Hayashi, Thermally initiated detonation through deflagration to detonation transition, Proceedings of the Royal Society of London. Series A: Mathematical and Physical Sciences 435 (1895) (1991) 459–482. doi:https://doi.org/10.1098/rspa.1991.0156.

[8] D. Jones, G. Kemister, R. Borg, Numerical Simulation of Detonation in Condensed Phase explosives, Tech. rep., Weapons Systems Division. Aeronautical and Maritime Research Laboratory. DSTO-TR-0705. Department of Defence. Defence Science and Technology Organisation. PO Box 43331, Melbourne Victoria 3001 Australia (1999).

[9] M. Arienti, E. Morano, J. Shepherd, Shock and detonation modeling with the Mie-Grüneisen equation of state, Tech. rep., Graduate Aeronautical Laboratories Report FM99-8, California Institute of Technology, Pasadena, CA (2004).

[10] C. Tarver, Ignition and Growth Modeling of LX-17 Hockey Puck Experiments, Propellants, Explosives, Pyrotechnics 30 (2) (2005) 109–117. doi:https://doi.org/10.1002/prep.200400092.

[11] D. Schwendeman, A. Kapila, W. Henshaw, A Comparative Study of Two Macro-Scale Models of Condensed-Phase Explosives, IMA Journal of Applied Mathematics 1 (2005) 17. doi:https://doi.org/10.1093/imamat/hxr078.

[12] G. DeOliveira, A. Kapila, D. Schwendeman, J. Bdzil, W. Henshaw, C. Tarver, Detonation diffraction, dead zones, and the ignition-and-growth model, in: The Thirteenth Symposium (International) on Detonation, Vol. 16, 2006.

[13] A. Kapila, D. Schwendeman, J. Bdzil, W. Henshaw, A study of detonation diffraction in the ignition-and-growth model, Combustion Theory and Modelling 11 (5) (2007) 781–822. doi:https://doi.org/10.1080/13647830701235774.

[14] D. Kassoy, J. Kuehn, M. Nabity, J. Clarke, Detonation initiation on the microsecond time scale: DDTs, Combustion Theory and Modelling 12 (6) (2008) 1009–1047. doi:https://doi.org/10.1080/13647830802045080.

[15] J. Regele, D. Kassoy, M. Aslani, O. Vasilyev, Evolution of detonation formation initiated by a spatially distributed, transient energy source, Journal of Fluid Mechanics 802 (2016) 305–332. doi:https://doi.org/10.1017/jfm.2016.456.

[16] A. Autodyn, Theory manual revision 4.3., Century Dynamics, Concord, CA, Livermore Software Technology Corporation (LSTC) (2005).

[17] A. A. C. Livermore Software Technology (LST), LS-DYNA Keyword users's manual Volume I LS-DYNA R13, Livermore, California (2021).

[18] Y. Zeldovich, On the theory of the propagation of detonation in gaseous system, J. of. Experimental and Theoretical Physics of the U.S.S.R. 10 (1940) 542–568.

[19] J. Von Neumann, Theory of Detonation Waves, Office of Science Research Development (1942) Report No. 549.

[20] W. Doering, Beitrage zur Theorie der Detonation, Ann. Physik 43 (1943) 421–428.

[21] E. Lee, H. Hornig, J. Kury, Adiabatic expansion of high explosive detonation products, Tech. rep., Univ. of California Radiation Lab. at Livermore, Livermore, CA (United States) (1968). doi:https://doi.org/10.2172/4783904.

[22] R. Menikoff, JWL equation of state, No. LA-UR-15-29536, Tech. rep., Los Alamos National Lab. (LANL), Los Alamos, NM (United States) (2015). doi:https://doi.org/10.2172/1229709.

[23] S. Godunov, A. Zabrodine, M. Ivanov, A. Kraïko, G. Prokopov, V. Platonov, Résolution numérique des problèmes multidimensionnels de la dynamique des gaz, Éditions Mir (Moscou), 1979.

[24] R. Menikoff, B. Plohr, The Riemann problem for fluid flow of real materials, Reviews of modern physics 61 (1) (1989) 75. doi:https://doi.org/10.1103/RevModPhys.61.75.

[25] A. Chiapolino, R. Saurel, Extended Noble-Abel Stiffened-Gas Equation of State for Sub-and-Supercritical Liquid-Gas Systems Far from the Critical Point, Fluids 3 (48) (2018). doi:https://doi.org/10.3390/fluids3030048.

[26] L. Neron, R. Saurel, Noble–Abel/first-order virial equations of state for gas mixtures resulting from multiple condensed reactive materials combustion, Physics of Fluids 34 (1) (2022) 016107. doi:https://doi.org/10.1063/5.0079187.

[27] L. Neron, R. Saurel, A. Chiapolino, F. Fraysse, Relaxation method for Mie-Grüneisen type equations of state, Physics of Fluids 35 (11) (2023) 116112. doi:https://doi.org/10.1063/5.0169781.

[28] R. Saurel, F. Petitpas, R. Berry, Simple and efficient relaxation methods for interfaces separating compressible fluids, cavitating flows and shocks in multiphase mixtures, Journal of Computational Physics 228 (5) (2009) 1678–1712. doi:https://doi.org/10.1016/j.jcp.2008.11.002.

[29] O. Le Métayer, R. Saurel, The Noble-Abel Stiffened-Gas equation of state, Physics of Fluids 28 (4) (2016) 046102. doi:https://doi.org/10.1063/1.4945981.

[30] A. Chiapolino, R. Saurel, B. Nkonga, Sharpening diffuse interfaces with compressible fluids on unstructured meshes, Journal of Computational Physics 340 (2017) 389–417. doi:https://doi.org/10.1016/j.jcp.2017.03.042.

[31] R. Saurel, C. Pantano, Diffuse Interfaces and Capturing Methods in Compressible Two-Phase Flows, Annual Review of Fluid Mechanics 50 (2018) (2018) 105–130. doi:https://doi.org/10.1146/annurev-fluid-122316-050109.

[32] T. Liu, Hyperbolic conservation laws with relaxation, Communications in Mathematical Physics 108 (1987) 153–175. doi:https://doi.org/10.1007/BF01210707.

[33] S. Godunov, A. Zabrodine, M. Ivanov, A. Kraïko, G. Prokopov, Numerical solution of multidimensional problems of gas dynamics, Moscow Izdatel Nauka, 1976.

[34] B. Plohr, Shockless acceleration of thin plates modeled by a tracked random choice method, AIAA journal 26 (4) (1988) 470–478. doi:https://doi.org/10.2514/3.9917.

[35] R. Saurel, R. Abgrall, A simple method for compressible multifluid flows, SIAM Journal on Scientific Computing 21 (3) (1999) 1115–1145. doi:https://doi.org/10.1137/S1064827597323749.

[36] O. Anderson, Equations of state of solids for geophysics and ceramic science, no. 31, Oxford University Press, USA, 1995.

[37] E. Lozano, M. Cawkwell, T. Aslam, An analytic and complete equation of state for condensed phase materials, Journal of Applied Physics 134 (12) (2023) 125102. doi:https://doi.org/10.1063/5.0165249.

[38] F. Stacey, J. Hodgkinson, Thermodynamics with the Grüneisen parameter: Fundamentals and applications to high pressure physics and geophysics, Physics of the Earth and Planetary Interiors 286 (2019) 42–68. doi:https://doi.org/10.1016/j.pepi.2018.10.006.

[39] O. Le Métayer, J. Massoni, R. Saurel, Dynamic relaxation processes in compressible multiphase flows. Application to evaporation phenomena, in: ESAIM: Proceedings, Vol. 40, EDP Sciences, 2013, pp. 103–123. doi:https://doi.org/10.1051/proc/201340007.

[40] S. Godunov, A finite difference scheme for numerical computation of the discontinuous wave solutions of equations of fluid dynamics, Math. Sb. 47 (1959) 271–306.

[41] R. Saurel, E. Franquet, E. Daniel, O. Le Métayer, A relaxation-projection method for compressible flows. Part I: The numerical equation of state for the Euler equations, Journal of Computational Physics 223 (2) (2007) 822–845. doi:https://doi.org/10.1016/j.jcp.2006.10.004.

[42] R. Saurel, M. Larini, J. Loraud, Exact and approximate riemann solvers for real gases, Journal of Computational Physics 112 (1) (1994) 126–137. doi:https://doi.org/10.1006/jcph.1994.1086.

[43] J. Massoni, R. Saurel, A. Lefrançois, G. Baudin, Modeling spherical explosions with aluminized energetic materials, Shock Waves 16 (1) (2006) 75–92. doi:https://doi.org/10.1007/s00193-006-0053-y.

[44] A. Chiapolino, P. Boivin, R. Saurel, A simple and fast phase transition relaxation solver for compressible multicomponent two-phase flows, Computers & Fluids 150 (2017) 31–45. doi:https://doi.org/10.1016/j.compfluid.2017.03.022.

[45] J. Johnson, P. Tang, C. Forest, Shock-wave initiation of heterogeneous reactive solids, Journal of Applied Physics 57 (9) (1985) 4323–4334. doi:https://doi.org/10.1063/1.334591.

[46] R. Menikoff, M. Shaw, Reactive burn models ans ignition & growth concept, in: EPJ Web of Conferences, Vol. 10, 2010. doi:https://doi.org/10.1051/epjconf/20101000003.

[47] R. Saurel, F. Petitpas, R. Abgrall, Modelling phase transition in metastable liquids: application to cavitating and flashing flows, Journal of Fluid Mechanics 607 (2008) 313–350. doi:https://doi.org/10.1017/S0022112008002061.

[48] L. Fried, W. Howard, P. Souers, Kinetic modeling of non-ideal explosives with CHEETAH, Tech. rep., Lawrence Livermore National Lab. (LLNL), Livermore, CA (United States) (1998).

[49] J. Lu, Evaluation of the thermochemical code-CHEETAH 2.0 for modelling explosives performance, DSTO Aeronautical and Maritime Research Laboratory Edinburgh, 2001.

[50] W. Fickett, W. Davis, Detonation: theory and experiment, University of California Press, Berkeley, CA, 1979.

[51] V. Kogan, P. Levashov, I. Lomov, A. Bushman, I. Lomonosov, K. Khishchenko, V. Kopyshev, E. Kuzmenkov, Shock wave Database, Chernogolovka, Russia.
URL www.ihed.ras.ru/rusbank/

[52] A. Chiapolino, F. Fraysse, R. Saurel, A Method to Solve Hamilton-Jacobi Type Equation on Unstructured Meshes, Journal of Scientific Computing 88 (1) (2021) 1–43. doi:https://doi.org/10.1007/s10915-021-01517-9.

[53] R. Becker, Stosswelle und detonation, Zeitschrift für Physik 8 (1) (1922) 321–362. doi:https://doi.org/10.1007/BF01329605.

[54] G. Kistiakowsky, E. Wilson, The hydrodynamic theory of detonation and shock waves, Office of the Publication Board, Department of Commerce, 1941.

[55] R. Cowan, W. Fickett, Calculation of the detonation properties of solid explosives with the kistiakowsky-wilson equation of state, The Journal of Chemical Physics 24 (5) (1956) 932–939. doi:https://doi.org/10.1063/1.1742718.

[56] L. Neron, R. Saurel, Revisiting the Becker-Kistiakowsky-Wilson equation of state, Journal of Computational Physics 513 (2024) 113165. doi:https://doi.org/10.1016/j.jcp.2024.113165.